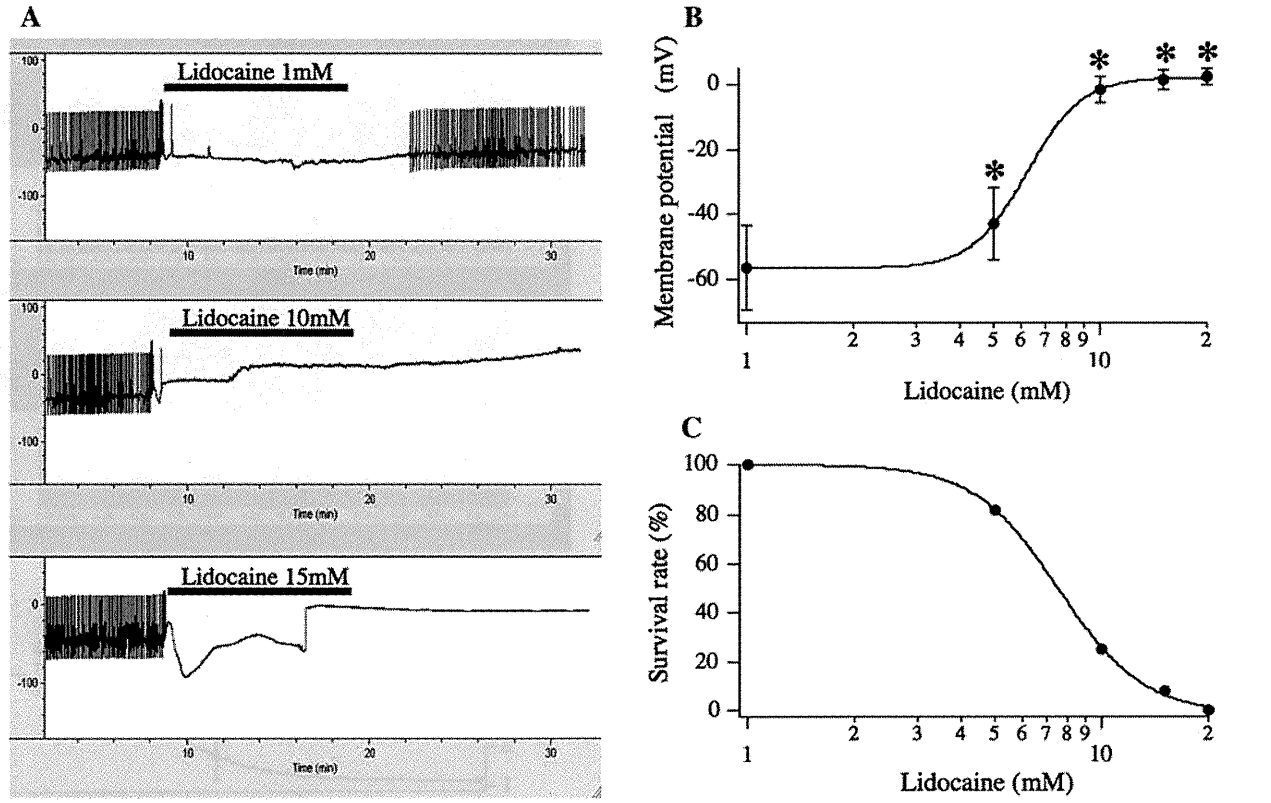

Fig. 2 **a** Lidocaine exposure greater than 10 mM for 10 min induced irreversible depolarization. **b** Graph shows the resting membrane potential of an LPeD1 cell. Lidocaine greater than 10 mM irreversibly depolarized membrane potential toward 0 mV. Results are presented as mean ± SD, $n = 6$ in each concentration. $^*P < 0.05$ in comparison to baseline values. **c** Survival rate of an LPeD1 cell after lidocaine exposure for 10 min at each concentration

Membrane resistance and capacitance measurement

Whole-cell membrane resistance and capacitance were measured by the whole-cell patch-clamp method. Figure 3a shows the experimental tracings of membrane resistance (upper trace) and capacitance (lower trace) before and after 10 mM lidocaine administration. Following lidocaine perfusion, membrane resistance was significantly decreased by 10 and 20 mM lidocaine: whole-membrane resistance changed from 1.4 ± 0.2 (GΩ) at the baseline to 1.2 ± 0.2 at 1 mM, 1.1 ± 0.2 at 5 mM, 0.5 ± 0.2 at 10 mM, 0.3 ± 0.1 at 15 mM, and 0.3 ± 0.2 at 20 mM, with a half-maximal response at 8.0 mM (Fig. 3b). In contrast, whole-membrane capacitance was significantly increased by 10 and 20 mM lidocaine, from 226 ± 52 (pF) at the baseline to 234 ± 54 at 1 mM, 244 ± 57 at 5 mM, 279 ± 66 at 10 mM, 294 ± 30 at 15 mM, and 301 ± 34 at 20 mM, with a half-maximal response at 7.7 mM (Fig. 3c).

Double staining with propidium iodide and annexin V-FITC

Figure 4a shows double staining with propidium iodide and Annexin V-FITC and imaging of an LPeD1 neuron before and after 10 mM lidocaine administration. The fluorescence of propidium iodide was increased faster than that of annexin V-FITC (Fig. 4a). In both propi dium iodide and annexin V-FITC, the fluorescent intensity level was significantly increased after lidocaine exposure for 10 min in a concentration-dependent manner (Fig. 4b). For propidium iodide (PI) staining, ED_{50} was 7.1 mM; for annexin V staining, ED_{50} was 7.2 mM.

Discussion

In the present study, lidocaine induced morphological swelling and irreversible depolarization in a neuron (Figs. 1, 2). To demonstrate whether lidocaine induced membrane destruction, membrane resistance and capacitance were measured. As measured by the whole-cell patch-clamp method, lidocaine decreased membrane resistance and increased capacitance (Fig. 3). Lidocaine induced staining for nucleic acid by propidium iodide, which is one of the markers of necrosis (Fig. 4). Lidocaine also induced phosphatidyl serine exhibition at the cell surface, a marker of early-stage apoptosis (Fig. 4). These

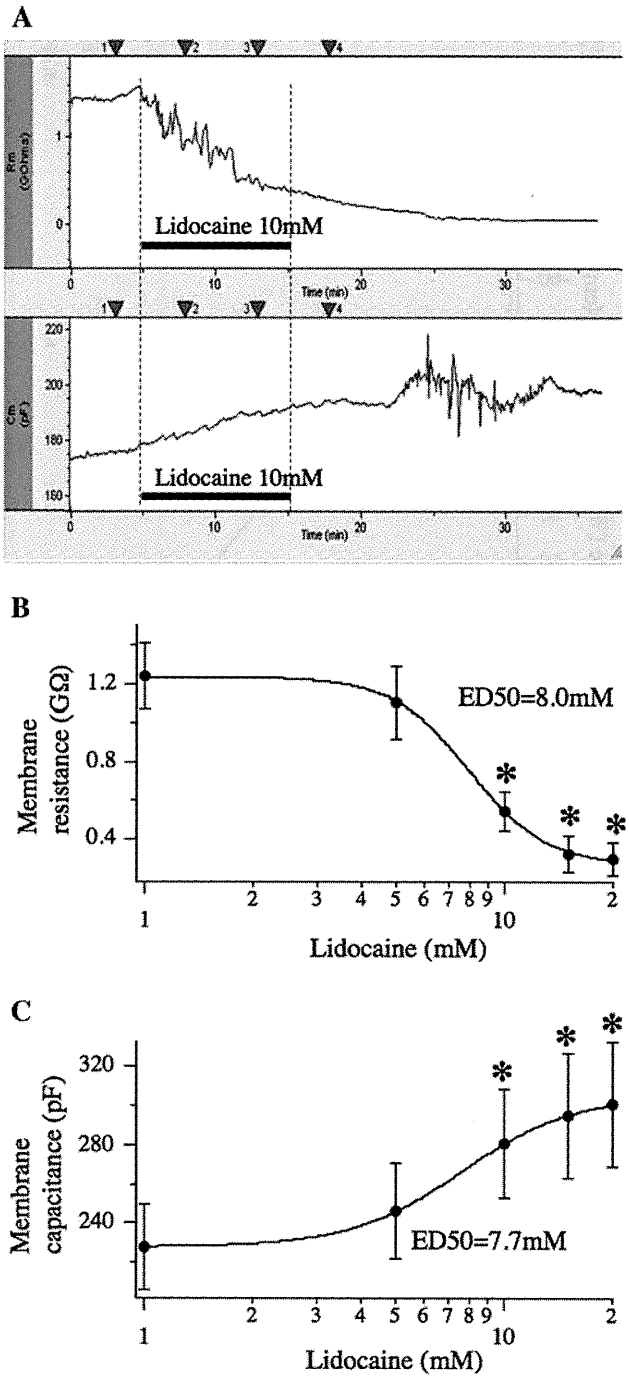

Fig. 3 **a** *Upper trace* shows that lidocaine exposure above 10 mM for 10 min decreased membrane resistance irreversibly. *Lower trace* shows that lidocaine exposure increased membrane capacitance irreversibly. **b** Graph of membrane resistance. Results are presented as mean ± SD, $n = 6$ in each concentration. $^*P < 0.05$ in comparison to baseline values. **c** Graph of membrane capacitance of an LPeD1 cell. Results are presented as mean ± SD, $n = 6$ in each concentration. $^*P < 0.05$ in comparison to baseline values

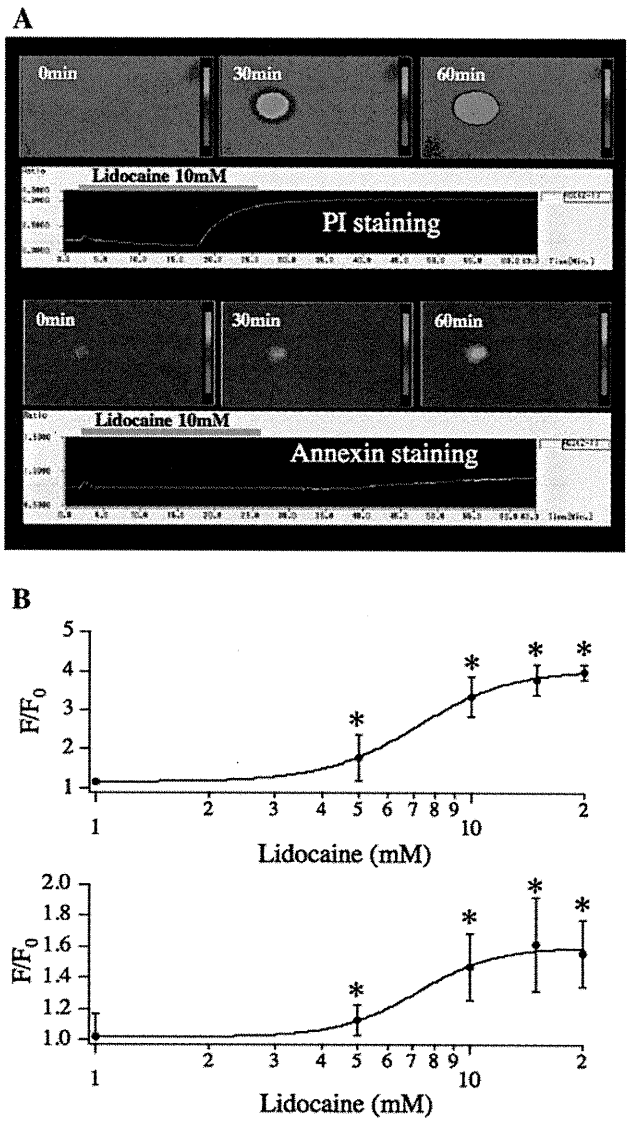

Fig. 4 **a** Fluorescence intensities of propidium iodide (*PI*) and *annexin* V-FITC were measured simultaneously. *Upper trace* and *graph* show fluorescence intensity of propidium iodide (PI); *lower trace* and *graph* show fluorescence intensity of annexin V-FITC before and after lidocaine exposure in the same LPeD1 cell. **b** *Upper graph* fluorescence intensity of PI; *lower graph* fluorescence intensity of annexin V-FITC. Results are presented as mean ± SD, $n = 6$ in each concentration. $^*P < 0.05$ in comparison to baseline values

results indicate that clinical doses of lidocaine at more than 5 mM destroy the cell membrane and induce both apoptosis and necrosis in a neuronal cell.

Many studies have indicated that local anesthetics, especially lidocaine, induce apoptosis or necrosis in neuronal cells, and many mechanisms for the cell toxicity of lidocaine have been investigated. Using frog sciatic nerve, Bainton and Strichartz demonstrated a reduction in compound action potential at 40 mM (1%) lidocaine, with complete ablation at 80 mM lidocaine after washout [29]. Similarly, Kanai et al. reported that a high concentration of lidocaine (80 mM) induced irreversible depolarization, and they concluded that lidocaine had a direct neurotoxic effect

on crayfish giant axons in vitro [30]. These findings suggest that a high concentration of lidocaine may induce transient or permanent neurological deficits, particularly in nerves already jeopardized by direct needle trauma during spinal anesthesia. Werdehausen et al. [8] compared the toxicity of local anesthetics by double-staining assay with 7-amino-actinomycin D (7-AAD) and annexin V measured by flow cytometry in the human neuroblastoma SK-N-SH cell line. They reported that local anesthetics induced about 20% apoptosis and that toxicity was correlated with octanol/buffer coefficients, indicating lipophilicity. Kamiya et al. [31] reported that below 12 mM, lidocaine exposure for 24 h induced about 50% apoptosis in U937 human leukemia cells. Friederich and Schmitz [32] reported that 24-h exposure to 3 mM lidocaine induced about 40% apoptosis in human neuronal SH-SY5Y cells. Lidocaine and mepivacaine exposure increased the number of apoptotic cells significantly more than other anesthetics. At a high concentration (greater than 5 mM), the number of necrotic cells increased. Although many theories have been reported, whether apoptosis or necrosis is primarily induced by lidocaine has been unclear. One reason is that in most of the studies of apoptosis by lidocaine, samples were obtained at 6–24 h after lidocaine exposure, making it difficult to determine whether apoptosis or necrosis was the primary occurrence. The current experiment is the first to provide evidence that lidocaine induces both apoptosis and necrosis in the same neuron within 60 min of lidocaine exposure.

It is generally accepted that cell death can result from either a passive degenerative process (necrosis) or an active process (apoptosis). A multitude of methods, each of them suitable to different experimental conditions, have been described to identify apoptotic cells by flow cytometric analysis [33]. Flow cytometry is the technique of choice for the quantification of apoptosis. One general problem that always arises with the flow cytometric analysis of apoptosis, however, is the distinction between necrotic and apoptotic cells. Moreover, although necrotic cells are usually thought to contaminate objects during the quantification of apoptosis, it is interesting to quantify both apoptosis and necrosis in a given cell population. Although there is no clear-cut parameter that allows the separation by flow cytometry of necrotic from apoptotic cells, particularly at their late stages, such a distinction is immediate with morphological techniques. The presence of apoptotic cells in a given population should always be validated by morphological observations. Therefore, morphological observations from different perspectives under a microscope are important for the identification of apoptosis and its distinction from necrosis.

In apoptotic cells, the membrane phospholipid phosphatidylserine (PS) is translocated from the inner to the outer leaflet of the plasma membrane, thereby exposing PS to the external cellular environment. Annexin V is a 35–36 kDa Ca^{2+}-dependent phospholipid-binding protein that has a high affinity for PS and binds to cells with exposed PS. Annexin V may be conjugated to fluorochromes, including fluorescein isothiocyanate (FITC). This format retains its high affinity for PS and thus serves as a sensitive probe for flow cytometric analysis of cells undergoing apoptosis. Because the externalization of PS occurs in the early stages of apoptosis, FITC annexin V staining can identify apoptosis at an earlier stage than assays based on nuclear changes such as DNA fragmentation. On the other hand, necrosis occurs when the cell membrane loses its integrity and becomes leaky. Therefore, necrotic cells are easily stained with propidium iodide.

Tsuchiya et al. [34] demonstrated that lidocaine induced inflammation through changes in membrane fluidity, supporting the theory of Kitagawa et al. [35] that cytotoxic local anesthetics are amphiphilic molecules that will melt lipid bilayers as detergents and induce necrosis. On the other hand, we previously reported that local anesthetics, especially lidocaine, increase intracellular pH, thus affecting homeostasis [10]. Mitochondria are especially affected and depolarized by intracellular pH changes and will trigger apoptosis or necrosis [36–38].

In the present study, the concentration of lidocaine was established for clinical use; however, lidocaine induced irreversible toxic effects. In clinical practice, 40–80 mM (1–2%) of lidocaine is used; therefore, a high concentration of lidocaine may accumulate in a local area and induce neurological damage. This discrepancy between experimentally effective concentrations for anesthetic actions and those for toxic doses must be considered: 10 mM lidocaine is considered to be a clinically acceptable concentration. Ross et al. and Rigler and Drasner [39, 40] reported that spinal injection with 5% lidocaine was diluted into 1–3% in a human spinal model; therefore, the lidocaine concentration used in this experiment is a potential concentration. Of course, cells are surrounded by fibers or sheaths; however, if lidocaine is injected into a sheath directly, a high concentration of lidocaine will remain in the vicinity of the nerve cells.

However, in attempting to transfer concentrations to the clinical setting, major problems with species differences may occur. The greatest difference between *Lymnaea* and mammals is that the *Lymnaea* has a very large central nervous system (150 μm) that is quite simple in comparison to that of a mammal. Major neurons were identified and named in each. Therefore, each target neuron can be picked up with the use of a micropipette. In addition, in *Lymnaea*, voltage-dependent sodium channels are mostly tetrodotoxin (TTX) resistant, but these *Lymnaea* neurons are blocked by local anesthetics at the same clinical concentration as in mammals [41].

Lymnaea neurons have a lipid bilayer structure that is similar to that in mammals. In addition, the LPeDl neuron has anesthetic-activated potassium currents, such as Ikir, produced by two-pore-domain background K^+ channels, such as TASK and TREK-1, the same as in mammal neurons. Therefore, the membrane potential of LPeD1 is hyperpolarized by general anesthetics in a clinical concentration [42–44].

In this experiment, we isolated and used the identified LPeD1 neuron as a respiratory pattern generator and demonstrated that it has a spontaneous action potential. This pacemaker neuron, similar to other respiratory pacemaker neurons, has a slowly inactivating component of the sodium current and can produce spontaneous action potentials continuously. Therefore, the membrane potential and conditions can be clearly observed for a long time. The major receptors and ion channels that have been identified in *Lymnaea* neurons are similar to those in humans; therefore, isolated and identified *Lymnaea* neurons represent an excellent model for the study of the effects of lidocaine [45, 46].

In conclusion, lidocaine irreversibly depolarizes the membrane potential and induces apoptosis and necrosis in a neuron.

Acknowledgments This work was supported in part by a Grant-in-Aid (No. 21591978) for Basic Scientific Research (C) from the Ministry of Education, Science, and Technology of Japan.

References

1. Lambert LA, Lambert DH. Irreversible conduction block in isolated nerve by high concentrations of local anesthetics. Anesthesiology. 1994;80:1082–93.
2. Rigler ML, Drasner K, Krejcie TC, Yelich SJ, Scholnick FT, DeFontes J, Bohner D. Cauda equina syndrome after continuous spinal anesthesia. Anesth Analg. 1991;72:275–81.
3. Drasner K. Model for local anesthetic toxicity from continuous spinal anesthesia. Reg Anesth. 1993;18:343–8.
4. Gerancher JC. Cauda equine syndrome following a single spinal administration of 5% hyperbaric lidocaine through a 25-gauge Whitacre needle. Anesthesiology. 1997;87:687–9.
5. Sakura S, Kirihara Y, Muguruma T, Kishimoto T, Saito Y. The comparative neurotoxicity of intrathecal lidocaine and bupivacaine in rats. Anesth Analg. 2005;101:541–7.
6. Kasaba T, Onizuka S, Takasaki M. Procaine and mepivacaine have less toxicity in vitro than other clinically used local anesthetics. Anesth Analg. 2003;9:85–90.
7. Onizuka S, Takasaki M, Syed NI. Long-term exposure to local but not inhalation anesthetics affects neurite regeneration and synapse formation between identified *Lymnaea* neurons. Anesthesiology. 2005;102:353–63.
8. Werdehausen R, Braun S, Essmann F, Schulze-Osthoff K, Walczak H, Lipfert P, Stevens MF. Lidocaine induces apoptosis via the mitochondrial pathway independently of death receptor signaling. Anesthesiology. 2007;107:136–43.
9. Johnson ME, Uhl CB, Spittler KH, Wang H, Gores GJ. Mitochondrial injury and caspase activation by the local anesthetic lidocaine. Anesthesiology. 2004;101:1184–94.
10. Onizuka S, Tamura R, Hosokawa N, Kawasaki Y, Tsuneyoshi I. Local anesthetics depolarize mitochondrial membrane potential by intracellular alkalization in rat dorsal root ganglion neurons. Anesth Analg. 2010;111:775–83.
11. Onizuka S, Yonaha T, Tamura R, Kashiwada M, Shirasaka T, Tsuneyoshi I. Lidocaine depolarize mitochondrial membrane potential by intracellular alkalization in rat dorsal root ganglion neurons. J Anesth. 2011;25:229–39.
12. Onizuka S, Kasaba T, Hamakawa M, Ibusuki I, Takasaki M. Lidocaine increases intracellular sodium concentration through voltage-dependent sodium channels in an identified *Lymnaea* neuron. Anesthesiology. 2004;101:110–9.
13. Yagiela JA, Benoit PW, Fort NF. Mechanism of epinephrine enhancement of lidocaine-induced skeletal muscle necrosis. J Dent Res. 1982;61:686–90.
14. Lawrence VS, Marte E, Brown BW, Van Bergen FH. Lidocaine, 2-chlorprocaine and hepatic necrosis. Anesth Analg. 1966;45:55–8.
15. Howl JD, Publicover SJ. Bay K 8644 induced necrosis in murine skeletal muscle in vitro: myofibre breakdown precedes significant alterations of intracellular [Ca] or pH. Acta Neuropathol. 1989;77:634–44.
16. Arrebola F, Zabiti S, Cañizares FJ, Cubero MA, Crespo PV, Fernández-Segura E. Changes in intracellular sodium, chlorine, and potassium concentrations in staurosporine-induced apoptosis. J Cell Physiol. 2005;204:500–7.
17. Belaud-Rotureau MA, Leducq N, Poulletier Macouillard, de Gannes F, Diolez P, Lacoste L, Lacombe F, Bernard P, Belloc F. Early transitory rise in intracellular pH leads to Bax conformation change during ceramide-induced apoptosis. Apoptosis. 2000;5:551–60.
18. Sebbagh M, Renvoizé C, Hamelin J, Riché N, Bertoglio J, Bréard J. Caspase-3-mediated cleavage of ROCK I induces MLC phosphorylation and apoptotic membrane blebbing. Nat Cell Biol. 2001;3:346–52.
19. Chen T, Wang J, Xing D, Chen WR. Spatio-temporal dynamic analysis of bid activation and apoptosis induced by alkaline condition in human lung adenocarcinoma cell. Cell Physiol Biochem. 2007;20:569–78.
20. Yang KT, Pan SF, Chien CL, Hsu SM, Tseng YZ, Wang SM, Wu ML. Mitochondrial Na^+ overload is caused by oxidative stress and leads to activation of the caspase 3-dependent apoptotic machinery. FASEB J 2004;18:1442–4.
21. Van Cruchten S, Van Den Broeck W. Morphological and biochemical aspects of apoptosis, oncosis and necrosis. Anat Histol Embryol. 2002;31:214–23.
22. Doonan F, Cotter TG. Morphological assessment of apoptosis. Methods. 2008;44:200–4.
23. Syed N, Bulloch A, Lukowiak K. In vitro reconstruction of the respiratory central pattern generator of the mollusk *Lymnaea*. Science. 1990;12:282–5.
24. Tchoukalova YD, Harteneck DA, Karwoski RA, Tarara J, Jensen MD. A quick, reliable, and automated method for fat cell sizing. J Lipid Res. 2003;44:1795–801.
25. Brierley MJ, Staras K, Benjamin PR. Behavioral function of glutamatergic interneurons in the feeding system of *Lymnaea*. J Neurophysiol. 1997;78:3386–95.
26. Kits KS, Lodder JC, Veerman MJ. Phe-Met-Arg-Phe-amide activates a novel voltage-dependent K^+ current through a lipoxygenase pathway in molluscan neurons. J Gen Physiol. 1997;110:611–28.
27. Sakakibara M, Okuda F, Nomura K, Watanabe K, Meng H, Horikoshi T, Lukowiak K. Potassium currents in isolated statocyst neurons and RPeD1 in the pond snail, *Lymnaea stagnalis*. J Neurophysiol. 2005;94:3884–92.
28. Hong JR, Lin TL, Hsu YL, Wu JL. Apoptosis precedes necrosis of fish cell line with infectious pancreatic necrosis virus infection. Virology. 1998;250:76–84.

29. Bainton CR, Strichartz CR. Concentration dependence of lidocaine-induced irreversible conduction loss in frog nerve. Anesthesiology. 1994;81:657–67.
30. Kanai Y, Katsuki H, Takasaki M. Graded, irreversible changes in crayfish giant axon as manifestations of lidocaine neurotoxicity in vitro. Anesth Analg. 1998;86:569–73.
31. Kamiya Y, Ohta K, Kaneko Y. Lidocaine-induced apoptosis and necrosis in U937 cells depending on its dosage. Biomed Res. 2005;26:231–9.
32. Friederich P, Schmitz TP. Lidocaine-induced cell death in a human model of neuronal apoptosis. Eur J Anaesthesiol. 2002;19:564–70.
33. Wlodkowic D, Skommer J, Darzynkiewicz Z. Flow cytometry-based apoptosis detection. Methods Mol Biol. 2009;559:19–32.
34. Tsuchiya H, Mizogami M, Ueno T, Takakura K. Interaction of local anaesthetics with lipid membranes under inflammatory acidic conditions. Inflammopharmacol. 2007;15:164–70.
35. Kitagawa N, Oda M, Totoki T. Possible mechanism of irreversible nerve injury caused by local anesthetics: detergent properties of local anesthetics and membrane disruption. Anesthesiology. 2004;100:962–7.
36. Brooks C, Ketsawatsomkron P, Sui Y, Wang J, Wang CY, Yu FS, Dong Z. Acidic pH inhibits ATP depletion-induced tubular cell apoptosis by blocking caspase-9 activation in apoptosome. Am J Physiol Renal Physiol. 2005;289:410–9.
37. Lagadic-Gossmann D, Huc L, Lecureur V. Alterations of intracellular pH homeostasis in apoptosis: origins and roles. Cell Death Differ. 2004;11:953–61.
38. Kim JM, Bae HR, Park BS, Lee JM, Ahn HB, Rho JH, Yoo KW, Park WC, Rho SH, Yoon HS, Yoo YH. Early mitochondrial hyperpolarization and intracellular alkalinization in lactacystin-induced apoptosis of retinal pigment epithelial cells. J Pharmacol Exp Ther. 2003;305:474–81.
39. Ross BK, Coda B, Heath CH. Local anesthetic distribution in a spinal model: a possible mechanism of neurologic injury after continuous spinal anesthesia. Reg Anesth. 1992;17:69–77.
40. Rigler ML, Drasner K. Distribution of catheter-injected local anesthetic in a model of the subarachnoid space. Anesthesiology. 1991;75:684–92.
41. Staras K, Győri J, Kemenes G. Voltage-gated ionic currents in an identified modulatory cell type controlling molluscan feeding. Eur J Neurosci. 2002;15:109–19.
42. Franks NP, Lieb WR. Stereospecific effects of inhalational general anesthetic optical isomers on nerve ion channels. Science. 1991;254:427–30.
43. Patel AJ, Honoré E, Lesage F, Fink M, Romey G, Lazdunski M. Inhalational anesthetics activate two-pore-domain background K+ channels. Nat Neurosci. 1999;2:422–6.
44. Lopes CM, Franks NP, Lieb WR. Actions of general anaesthetics and arachidonic pathway inhibitors on K^+ currents activated by volatile anaesthetics and FMRFamide in molluscan neurones. Br J Pharmacol. 1998;125:309–18.
45. Winlow W, Spencer GE, Syed NI, Qazzaz MM. Modulation of reconstructed peptidergic synapses and electrical synapses by general anaesthetics. Toxicol Lett. 1998;100:77–84.
46. Hamakawa T, Feng ZP, Grigoriv N, Inoue T, Takasaki M, Roth S, Lukowiak K, Hasan SU, Syed NI. Sevoflurane induced suppression of inhibitory synaptic transmission between soma–soma paired *Lymnaea* neurons. J Neurophysiol. 1999;82:2812–9.

J Anesth (2011) 25:609–613
DOI 10.1007/s00540-011-1167-7

SHORT COMMUNICATION

Effects of sevoflurane on voltage-gated sodium channel $Na_v1.8$, $Na_v1.7$, and $Na_v1.4$ expressed in *Xenopus* oocytes

Toru Yokoyama · Kouichiro Minami · Yuka Sudo · Takafumi Horishita · Junichi Ogata · Toshihiko Yanagita · Yasuhito Uezono

Received: 24 February 2011 / Accepted: 28 April 2011 / Published online: 8 June 2011

Abstract Sevoflurane is widely used as a volatile anesthetic in clinical practice. However, its mechanism is still unclear. Recently, it has been reported that voltage-gated sodium channels have important roles in anesthetic mechanisms. Much attention has been paid to the effects of sevoflurane on voltage-dependent sodium channels. To elucidate this, we examined the effects of sevoflurane on Na_v 1.8, Na_v 1.4, and Na_v 1.7 expressed in *Xenopus* oocytes. The effects of sevoflurane on Na_v 1.8, Na_v 1.4, and Na_v 1.7 sodium channels were studied by an electrophysiology method using whole-cell, two-electrode voltage-clamp techniques in *Xenopus* oocytes. Sevoflurane at 1.0 mM inhibited the voltage-gated sodium channels $Na_v1.8$, $Na_v1.4$, and $Na_v1.7$, but sevoflurane (0.5 mM) had little effect. This inhibitory effect of 1 mM sevoflurane was completely abolished by pretreatment with protein kinase C (PKC) inhibitor, bisindolylmaleimide I. Sevoflurane appears to have inhibitory effects on $Na_v1.8$, $Na_v1.4$, and Na_v 1.7 by PKC pathways. However, these sodium channels might not be related to the clinical anesthetic effects of sevoflurane.

Keywords Sevoflurane · Voltage-gated sodium channel · *Xenopus* oocytes

Electronic supplementary material The online version of this article (doi:10.1007/s00540-011-1167-7) contains supplementary material, which is available to authorized users.

T. Yokoyama · K. Minami (✉) · J. Ogata
Department of Anesthesiology and Critical Care Medicine, Jichi Medical University, Tochigi 329-0483, Japan
e-mail: kminami@med.uoeh-u.ac.jp

T. Yokoyama · K. Minami · Y. Sudo · Y. Uezono
Cancer Pathophysiology Division, National Cancer Center Research Institute, Tokyo, Japan

Y. Sudo
Department of Molecular and Cellular Biology, Nagasaki University School of Biomedical Sciences, Nagasaki, Japan

T. Horishita
Department of Anesthesiology, University of Occupational and Environmental Health, Kitakyushu, Japan

T. Yanagita
Department of Pharmacology, University of Miyazaki, School of Medicine, Miyazaki, Japan

Sevoflurane has commonly been used as an anesthetic in clinical practice. Until now, previous studies have examined the mechanisms of sevoflurane [1–4], but many aspects of the mechanism have remained unclear. Voltage-gated sodium channels play important roles in the action of potential initiation and propagation in excitable cells of nerve and muscle [5]. Recent reports have shown a relationship between volatile anesthetics and sodium channels [6–12], suggesting voltage-dependent sodium channels as a target of anesthetics. However, so far as sevoflurane is concerned, there has been little information on the functions of voltage-gated sodium channels.

$Na_v1.8$ is exclusively expressed in dorsal root ganglion (DRG) neurons that give rise to C- and Aδ-fibers [13, 14] and peripheral nerves [15], which play important roles in afferent pain pathways transmitting nociceptive signals to the spinal cord [14]. $Na_v1.7$ expresses in DRG, sympathetic nerves, and peripheral nerves and $Na_v1.4$ expresses in skeletal muscles and plays a role in action potential initiation and transmission in skeletal muscles [5]. Reflex of muscles and inhibition of sympathetic nerves are necessary during the operation. Thus, it would be interesting to study

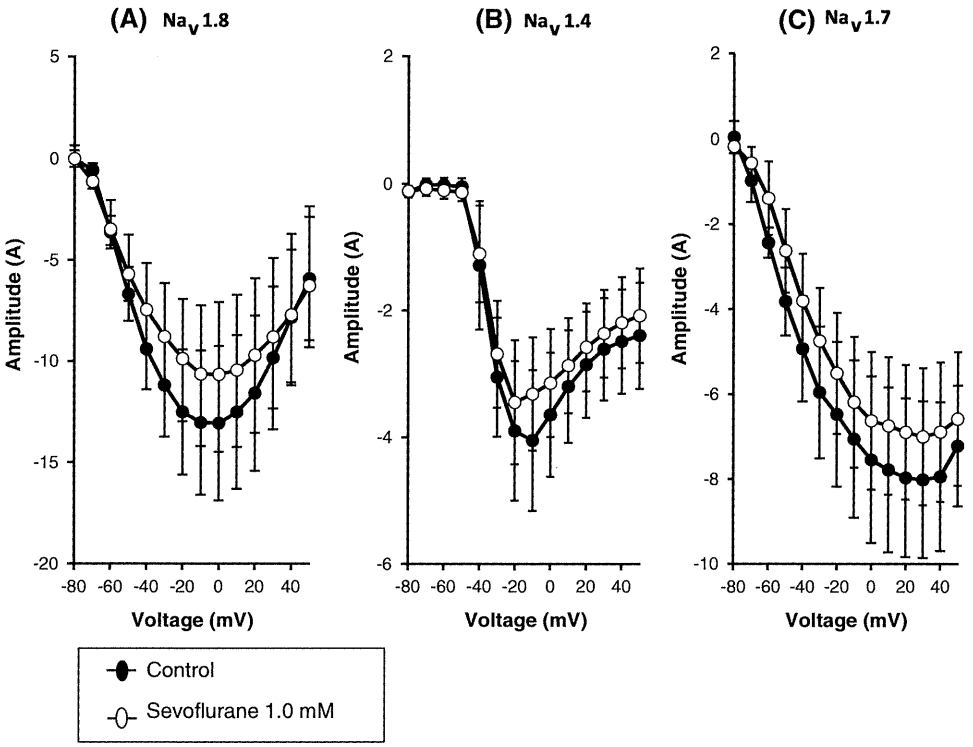

Fig. 1 Effects of sevoflurane on I–V relationship of sodium currents at holding potential of −70 mV: Na_v 1.8 (**a**), Na_v 1.4 (**b**), Na_v 1.7 (**c**). The peak currents were normalized to the maximal currents that were observed at −10 mV (Na_v 1.8 and Na_v1.4) and 30 mV (Na_v 1.7). *Closed circles*, control; *open circles*, sevoflurane

effects of sevoflurane on these voltage-dependent sodium channels.

The purpose of this study was to determine whether sevoflurane affects the functions of voltage-gated sodium channels. To this end, we examined the effects of sevoflurane on the function of Na_v1.7, Na_v1.8, and Na_v1.4 expressed in *Xenopus* oocytes using an electrophysiological method. Moreover, we investigated the mechanisms of the effects of sevoflurane on these channels.

Adult female *Xenopus laevis* frogs were purchased from Kato Kagaku (Tokyo, Japan), sevoflurane from Maruishi Pharmaceutical (Osaka, Japan), and bisindolylmaleimide I (GF109203X) from Calbiochem (La Jolla, CA, USA). Ultracomp *E. coli* Transformation Kit was purchased from Invitrogen (San Diego, CA, USA). Purification of cDNAs was performed with a Qiagen purification kit (Qiagen, Chatworth, CA, USA). Gentamicin, sodium pyruvate, cDNA for rat Na_v1.6 α-subunit (a gift from Dr. A.L. Goldin, University of California, Irvine, CA, USA), cDNA for rat Na_v1.8 α-subunit (a gift from Dr. A.N. Akopian, University of Texas Health Science Center, San Antonio, TX, USA), and cDNA for human Na_v1.7 α-subunit (a gift from Dr. F. Hofmann, Universität München, München, Germany) were prepared.

Each of the cRNAs (Na_v1.7, Na_v1.8, and Na_v1.4) was prepared using a mCAP mRNA Capping Kit and transcribed with a SP6 RNA Polymerase in vitro Transcription Kit (Ambion, Austin, TX, USA). cDNA was linearized with Na_v1.4, Na_v1.8, and Na_v 1.7. Preparation of *Xenopus laevis* oocytes and microinjection of the cRNA (Na_v1.7, Na_v1.8, and Na_v1.4) were performed as previously described by Horishita et al. [16, 17].

The whole-cell sodium current from oocytes was measured using a two-microelectrode voltage clamp. An oocyte was placed in a 100-μl recording chamber and perfused with frog Ringer's solution at room temperature (22°–24°C), containing 115 mM NaCl, 2.5 mM KCl, 10 mM HEPES, and 1.8 mM $CaCl_2$ at pH 7.2, at a rate of 1.8 ml/min using a perfusion pump (MINIPLUS3; GILSON, Middleton, France). The electrodes were triple-pulled with a puller (P-97; Sutter Instrument, Novoto, CA, USA) from a glass capillary. Microelectrodes were filled with 3 M KCl/0.5% low-melting-point agarose, and they had a final resistance of 0.3–0.5 MΩ. The whole-cell voltage clamp was achieved through these two electrodes using a Warner Instrument model OC-725C (Hampden, CT, USA). Currents were recorded and analyzed using pCLAMP software (Axon Instruments, Foster City, CA, USA). The voltage dependence activation was determined by eliciting 50-ms depolarizing pulses from a holding potential of −70 mV to potential range from −90 mV to 50 mV in 10-mV increments. We analyzed the peak component of the transient inward currents with methodology described by Horishita et al. [17]. A solution of sevoflurane, freshly prepared immediately before use, was applied for 2 min. We calculated the final concentration of sevoflurane in the recording chamber using gas chromatography. To determine whether activation of protein kinase C (PKC) plays a

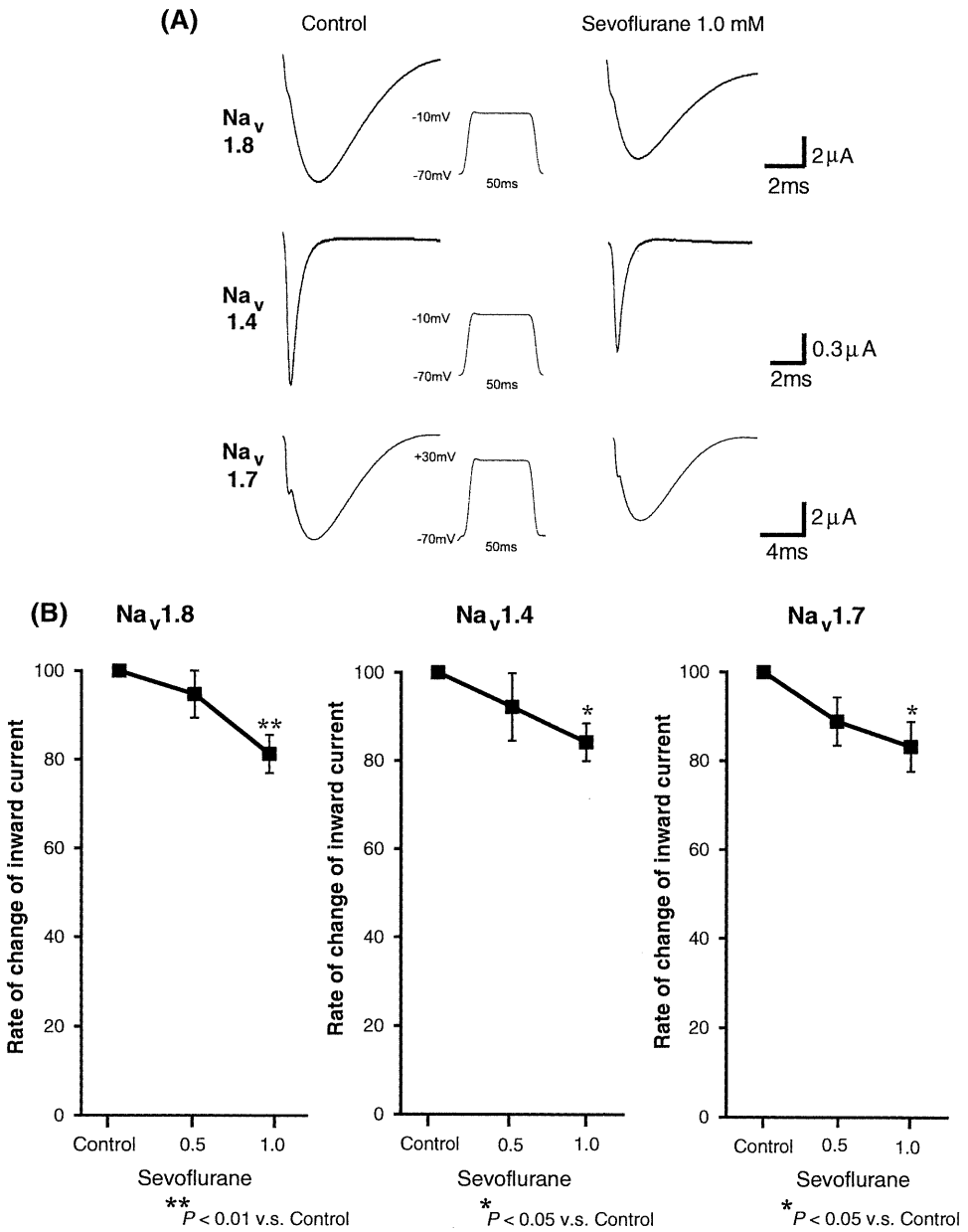

Fig. 2 Effects of sevoflurane on peak sodium currents in oocyte expressing Na_v 1.8, Na_v 1.4 and Na_v 1.7 expressed in *Xenopus* oocytes. **a** Representative I_{Na} traces in control and presence of sevoflurane in oocytes expressing Na_v1.8, Na_v 1.4, Na_v 1.7. **b** Concentration–response relationship of sevoflurane-induced inward current of voltage gated sodium channels. The effects were expressed as rate of change (± SEM). $*P < 0.05$, $**P < 0.01$ versus control

role in sevoflurane modulation on voltage-dependent sodium channels, oocytes were exposed to a PKC inhibitor, bisindolylmaleimide I (GF109203X)(200 nM) [18–20] in modified Barth's saline (MBS) for 120 min before recording. We compared the effects of sevoflurane on the peak component of the transient inward currents before and after the exposure to GF109203X.

Data are shown as the mean ± SEM. Results are expressed as percentages of control values obtained by peak current. The control responses were measured before sevoflurane application. Statistical analyses were performed using a one-way analysis of variance (ANOVA) and the Bonferroni correction using GraphPad Prism 4 (GraphPad Software, La Jolla, CA, USA). A P value <0.05 was considered significant.

Sevoflurane did not cause a shift in the current–voltage relationship (Fig. 1). Sevoflurane (1.0 mM) significantly inhibited the peak component of the transient inward currents of Na_v 1.8 (81.3% ± 4.32% of control, $P < 0.01$, $n = 8$), Na_v 1.4 (84.2% ± 4.35% of control, $P < 0.05$, $n = 12$), and Na_v 1.7 (83.2% ± 5.64% of control, $P < 0.05$, $n = 5$) (Figs. 1, 2). However, 0.5 mM sevoflurane had little effect on the peak component of the transient inward currents of these channels.

We next studied the effects of PKC on the inhibition of a high concentration of sevoflurane (1 mM) on Na_v 1.8, Na_v

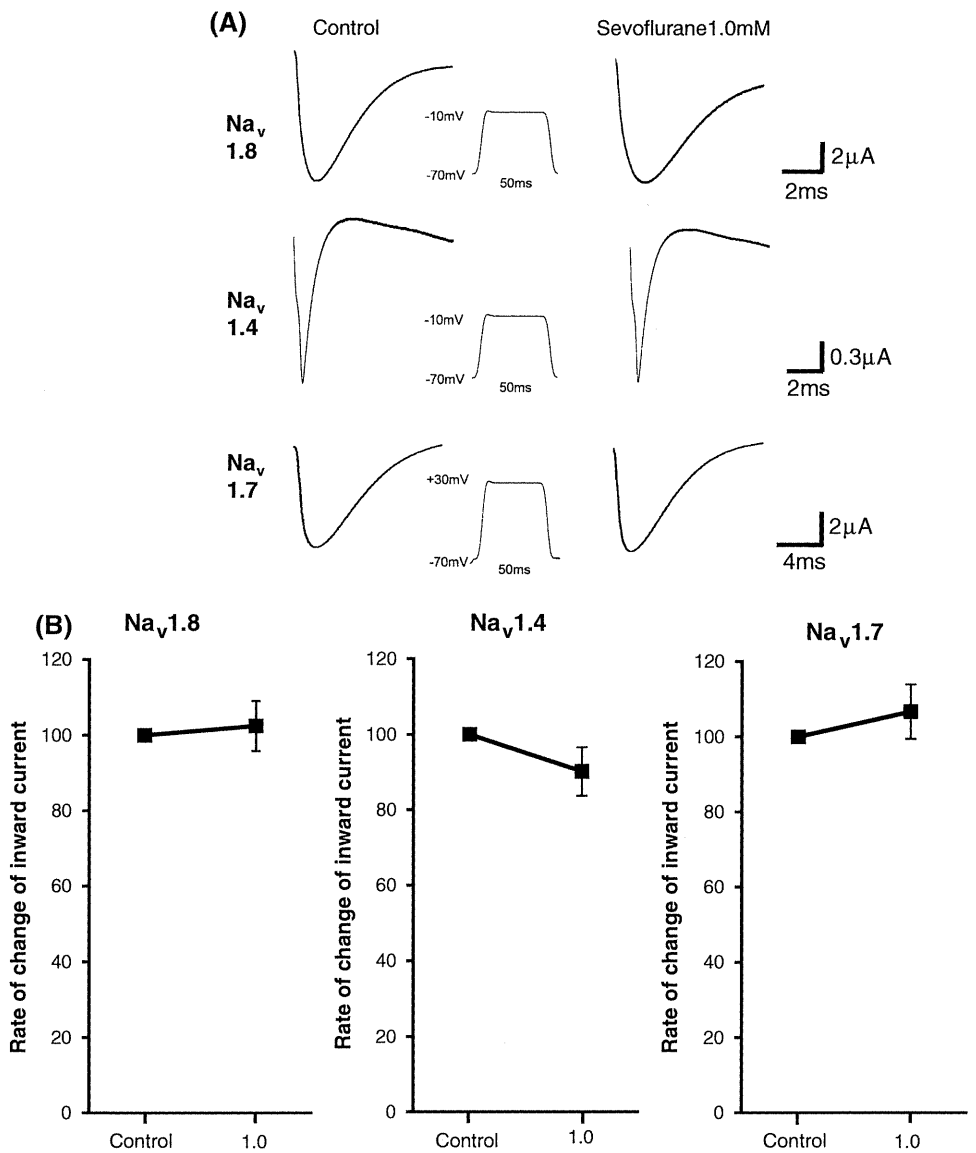

Fig. 3 Sevoflurane modulates voltage-gated sodium channels through the protein kinase C pathway. **a** Representative examples of the effect of bisindolylmaleimide I (GF109203X) on Na_v 1.8, Na_v 1.4 and Na_v 1.7. **b** Summary data for the effects of GF109203X on sevoflurane on peak inward current of voltage-gated sodium channels (Na_v 1.8, Na_v 1.4, and Na_v 1.7.). The effects were expressed as rate of change (± SEM)

1.4, and Na_v 1.7. In the control condition, the PKC inhibitor did not affect the voltage-gated inward currents. Pretreatment with GF109203X (200 nM) for 120 min abolished the sevoflurane-induced inhibition of voltage-evoked inward currents in *Xenopus* oocytes expressing $Na_v1.4$, $Na_v1.8$, and Na_v 1.7 ($Na_v1.4$, 90.2% ± 6.5% of control, $P > 0.05$, $n = 9$; $Na_v1.8$, 102% ± 6.6% of control, $P > 0.05$, $n = 11$; Na_v 1.7, 106% ± 7.2% of control, $P > 0.05$, $n = 9$) (Fig. 3a,b).

In our results, sevoflurane had little effects on the current–voltage relationship. However, sevoflurane (1.0 mM) significantly inhibited the peak component of the transient inward currents of Na_v 1.8, Na_v 1.4, and Na_v 1.7; 0.5 mM sevoflurane did not affect the peak component of the transient inward currents inward current of these three channels. In clinical situations, the free plasma concentration of sevoflurane is approximately 0.5 mM in humans [21, 22]. Ouyang et al. [12] reported that the function of $Na_v1.4$ was inhibited slightly by equipotent concentrations of sevoflurane (0.46 mM), consistent with our present results. From this evidence and our results, sevoflurane would have little effect on these channels, at least in a clinical situation.

In our present results, 1 mM sevoflurane inhibited the peak component of the transient inward currents of Na_v 1.8, Na_v 1.4, and Na_v 1.7. This finding raises the question of how sevoflurane inhibits these channel functions. Sodium channels are also rapidly phosphorylated by PKC [23], and recent reports have shown that the functions of Na_v 1.7 expressed in *Xenopus* oocytes are modulated by PKC [24]. Moreover, there are several lines of evidence revealing that sevoflurane activated PKC [2, 3]. Inhibition by sevoflurane on Na_v 1.8, Na_v 1.7, and Na_v 1.4 functions was abolished by pretreatment with the PKC inhibitor,

suggesting that sevoflurane would inhibit Na_v 1.8, Na_v 1.7, and Na_v 1.4 functions by PKC-mediated pathways.

In conclusion, we demonstrated inhibition by sevoflurane on the functions of Na_v 1.8, Na_v 1.7, and Na_v 1.4, and that the inhibition would be mediated by the PKC pathway. However, these sodium channels might not be related to the clinical anesthetic effects of sevoflurane.

Acknowledgments This study was supported by a Grant-in-Aid for Scientific Research on Scientific Research (C) No. 20602019 and No. 23590282 (T. Y.), No. 23592263 (J. O.) and No. 23592264 (K. M.) from the Ministry of Education, Culture, Sports, Science and Technology, Japan.

References

1. Lee SA, Choi JG, Zuo Z. Volatile anesthetics attenuate oxidative stress-reduced activity of glutamate transporter type 3. Anesth Analg. 2009;109:1506–10.
2. Hasegawa J, Takekoshi S, Nagata H, Osamura RY, Suzuki T. Sevoflurane stimulates MAP kinase signal transduction through the activation of PKC alpha and beta II in fetal rat cerebral cortex cultured neuron. Acta Histochem Cytochem. 2006;39:163–72.
3. Bouwman RA, van't Hof FN, de Ruijter W, van Beek-Harmsen BJ, Musters RJ, de Lange JJ, Boer C. The mechanism of sevoflurane-induced cardioprotection is independent of the applied ischaemic stimulus in rat trabeculae. Br J Anaesth. 2006; 97:307–14.
4. Yasui Y, Masaki E, Kato F. Sevoflurane directly excites locus coeruleus neurons of rats. Anesthesiology. 2007;107:992–1002.
5. Catterall WA, Goldin AL, Waxman SG. International Union of Pharmacology. XLVII. Nomenclature and structure–function relationships of voltage-gated sodium channels. Pharmacol Rev. 2005;57:397–409.
6. Ratnakumari L, Hemmings HC Jr. Inhibition of presynaptic sodium channels by halothane. Anesthesiology. 1998;88: 1043–54.
7. Ouyang W, Wang G, Hemmings HC Jr. Isoflurane and propofol inhibit voltage-gated sodium channels in isolated rat neurohypophysial nerve terminals. Mol Pharmacol. 2003;64:373–81.
8. Ratnakumari L, Vysotskaya TN, Duch DS, Hemmings HC Jr. Differential effects of anesthetic and nonanesthetic cyclobutanes on neuronal voltage-gated sodium channels. Anesthesiology. 2000;92:529–41.
9. Herold KF, Nau C, Ouyang W, Hemmings HC Jr. Isoflurane inhibits the tetrodotoxin-resistant voltage-gated sodium channel $Na_v1.8$. Anesthesiology. 2009;111:591–9.
10. Shiraishi M, Harris RA. Effects of alcohols and anesthetics on recombinant voltage-gated Na^+ channels. J Pharmacol Exp Ther. 2004;309:987–94.
11. Hemmings HC Jr. Sodium channels and the synaptic mechanisms of inhaled anaesthetics. Br J Anaesth. 2009;103:61–9.
12. Ouyang W, Herold KF, Hemmings HC Jr. Comparative effects of halogenated inhaled anesthetics on voltage-gated Na^+ channel function. Anesthesiology. 2009;110:582–90.
13. Akopian AN, Sivilotti L, Wood JN. A tetrodotoxin-resistant voltage-gated sodium channel expressed by sensory neurons. Nature. 1996;379:257–62.
14. Djouhri L, Fang X, Okuse K, Wood JN, Berry CM, Lawson SN. The TTX-resistant sodium channel $Na_v1.8$ (SNS/PN3): expression and correlation with membrane properties in rat nociceptive primary afferent neurons. J Physiol. 2003;550:739–52.
15. Gold MS, Weinreich D, Kim CS, Wang R, Treanor J, Porreca F, Lai J. Redistribution of Na(V)1.8 in uninjured axons enables neuropathic pain. J Neurosci. 2003;23:158–66.
16. Horishita T, Eger EI 2nd, Harris RA. The effects of volatile aromatic anesthetics on voltage-gated Na^+ channels expressed in *Xenopus* oocytes. Anesth Analg. 2008;107:1579–86.
17. Horishita T, Harris RA. *n*-Alcohols inhibit voltage-gated Na^+ channels expressed in *Xenopus* oocytes. J Pharmacol Exp Ther. 2008;326:270–7.
18. Toullec D, Pianetti P, Coste H, Bellevergue P, Grand-Perret T, Ajakane M, Baudet V, Boissin P, Boursier E, Loriolle F, Duhamel L, Charon D, Kirilovsky J. The bisindolylmaleimide GF 109203X is a potent and selective inhibitor of protein kinase C. J Biol Chem. 1991;266:15771–81.
19. Minami K, Minami M, Harris RA. Inhibition of 5-hydroxytryptamine type 2A receptor-induced currents by *n*-alcohols and anesthetics. J Pharmacol Exp Ther. 1997;281(3):1136–43.
20. Minami K, Gereau RW IV, Minami M, Heinemann SF, Harris RA. Effects of ethanol and anesthetics on type 1 and 5 metabotropic glutamate receptors expressed in *Xenopus laevis* oocytes. Mol Pharmacol. 1998;53:148–56.
21. Frink EJ Jr, Malan TP, Atlas M, Dominguez LM, DiNardo JA, Brown BR Jr. Clinical comparison of sevoflurane and isoflurane in healthy patients. Anesth Analg. 1992;74:241–5.
22. Holaday DA, Smith FR. Clinical characteristics and biotransformation of sevoflurane in healthy human volunteers. Anesthesiology. 1981;54:100–6.
23. Costa MR, Catterall WA. Phosphorylation of the alpha subunit of the sodium channel by protein kinase C. Cell Mol Neurobiol. 1984;4:291–7.
24. Vijayaragavan K, Boutjdir M, Chahine M. Modulation of $Na_v1.7$ and $Na_v1.8$ peripheral nerve sodium channels by protein kinase A and protein kinase C. J Neurophysiol. 2004;91:1556–69.

J Pharmacol Sci 115, 421 – 424 (2011)

Journal of Pharmacological Sciences

Short Communication

The Tramadol Metabolite *O*-Desmethyl Tramadol Inhibits Substance P–Receptor Functions Expressed in *Xenopus* Oocytes

Kouichiro Minami[1,2,*], Toru Yokoyama[1,2], Junichi Ogata[1], and Yasuhito Uezono[2]

[1]*Department of Anesthesiology and Critical Care Medicine, Jichi Medical University, Tochigi 329-0498, Japan*
[2]*Division of Cancer Pathophysiology, National Cancer Center Research Institute, Tokyo 104-0045, Japan*

Received December 6, 2010; Accepted January 25, 2011

Abstract. Tramadol has been widely used as analgesic. *O*-Desmethyl tramadol (ODT) is one of the main metabolites of tramadol, having much greater analgesic potency than tramadol itself. Substance P receptors (SPR) are well known to modulate nociceptive transmission within the spinal cord. In this study, we investigated the effects of ODT on SPR expressed in *Xenopus* oocytes by examining SP-induced Ca^{2+}-activated Cl^- currents. ODT inhibited the SPR-induced Cl^- currents at pharmacologically relevant concentrations. The protein kinase C (PKC) inhibitor bisindolylmaleimide I did not abolish the inhibitory effects of ODT on SP-induced Ca^{2+}-activated Cl^- currents. The results suggest that the tramadol metabolite ODT inhibits the SPR functions, which may be independent of activation of PKC-mediated pathways.

Keywords: *O*-desmethyl tramadol (ODT), tramadol, substance P

Substance P (SP) acts as a neurotransmitter released from C fibers located within nociceptive primary afferent neurons into the spinal cord and mediates a part of the excitatory synaptic input to nociceptive neurons at this level (1). SP and its receptors (SPR) are widely distributed in the central and peripheral nervous systems (2). Several studies showed that pain sensitivity is altered in mice lacking the gene encoding SPR; a reduction in nociceptive responses to certain somatic and visceral noxious stimuli occurs in SPR knockout mice (3).

SPR belongs to the family of Gq protein–coupled receptors that activate the protein kinase C (PKC) and Ca^{2+}-mobilization by stimulation of phospholipase C. Our recent reports have shown that the function of SPR is inhibited by volatile anesthetics and intravenous anesthetics. Halothane, isoflurane, enflurane, diethyl ether, and ethanol inhibit the function of SPR (4). Moreover, ketamine and pentobarbital inhibited the SPR-induced currents at pharmacologically relevant concentrations, whereas propofol had little effect on the currents in *Xenopus* oocytes expressing SPR (5). These results suggest that SPR is one of the targets of some anesthetics.

O-Desmethyl tramadol (ODT) is one of the metabolites of analgesic, tramadol. Only ODT among these metabolites has been shown to have analgesic activity in mice and rats, as assessed by the tail-flick responses. Analgesic potency of ODT is 2 – 4-times higher than that of tramadol (1, 3). In addition, ODT has more affinity for the μ-opioid receptor than does tramadol in biochemical receptor binding studies, although its chemical structure is quite similar to tramadol (1). There have been several reports suggesting that ODT, at pharmacologically relevant concentrations, inhibited 5-HT–evoked Ca^{2+}-activated Cl^- currents in oocytes expressing 5-HT_{2C}R, and inhibited the functions of NMDA receptors, but not those of glycine and $GABA_A$ receptors (6). We have previously reported in *Xenopus* oocytes expressing SPR that tramadol had little effect on the SP-induced Ca^{2+}-actvivated Cl^- currents (5). However, a recent report has shown that tramadol, given intraperitoneally or intravenously, produced significant inhibition of the biting behavior induced by intrathecal injection of SP (7). We have previously reported the different effects on the Gq-coupled muscarinic M_3 receptors (M_3R) between ODT and tramadol: tramadol inhibited acetylcholine (ACh)-induced currents in oocytes expressing M_3R, whereas ODT did not. In the report we suggest that ODT does not affect the M_3R-mediated signaling in spite of having only a small difference in its structure compared with that of tramadol (8). Collectively these data suggest that inhibitory effects of

*Corresponding author. kminami@med.uoeh-u.ac.jp
Published online in J-STAGE on March 2, 2011 (in advance)
doi: 10.1254/jphs.10313SC

tramadol on SP-induced biting behavior could be due to ODT, although the effects of ODT on SPR functions have not been studied in detail.

The *Xenopus* oocyte expression system has been used to study a multiplicity of receptors including Gq-coupled receptors (5). Stimulation of SPR results in activation of phospholipase C–mediated Ca^{2+}-activated Cl^- currents in *Xenopus* oocytes (4, 5). In the present study we examined the effects of the ODT on the SP-induced Ca^{2+}-activated Cl^- currents in SPR-expressing *Xenopus* oocytes.

Adult *Xenopus laevis* female frogs were purchased from Seac Yoshitomi (Yoshitomi, Fukuoka). SP was from Sigma (St. Louis, MO, USA). ODT hydrochloride was a kind gift from Nippon Shinyaku (Kyoto). Bisindolylmaleimide I (GF109203X) was from Calbiochem (La Jolla, CA, USA). The Ultracomp *E. coli* Transformation Kit was from Invitrogen (San Diego, CA, USA). A Qiagen (Chatsworth, CA, USA) Kit was used to purify plasmid cDNA. Rat SPR cDNA was kindly provided by Dr. J.E. Krause (Washington University School of Medicine, St. Louis, MO, USA). The cDNA for the SPR was inserted into the pBlueScriptIISK(−) vector and linearized with *Xba*I. The SPR synthetic RNA was prepared by using a mCAP mRNA Capping Kit and transcribed with a T7 RNA Polymerase in vitro Transcription Kit (Stratagene, La Jolla, CA, USA).

Isolation and microinjection of *Xenopus* oocytes were performed as described by Sanna et al. (9). Briefly, *Xenopus* oocytes were injected with 50 ng of synthetic RNA encoding SPR and incubated for 2 days. Oocytes were placed in a 100-μl recording chamber and perfused with modified Barth's saline (MBS) containing 88 mM NaCl, 1 mM KCl, 2.4 mM $NaHCO_3$, 10 mM HEPES, 0.82 mM $MgSO_4$, 0.33 mM $Ca(NO_3)_2$, and 0.91 mM $CaCl_2$ (pH 7.5) at a rate of 1.8 ml/min at room temperature. Recording and clamping electrodes (1 – 5 MΩ) were pulled from 1.2-mm outside diameter capillary tubing and filled with 3 M KCl. A recording electrode was imbedded in the animal's pole, and once the resting membrane potential stabilized, a clamping electrode was inserted and the resting membrane potential was allowed to restabilize. A Warner OC 725-B oocyte clamp (Hampden, CT, USA) was used to voltage-clamp each oocyte at −70 mV. We analyzed the peak of the transient inward current component of the SPR-induced currents because this component is dependent on SP concentration and is quite reproducible, as described by Minami et al. (4, 5). The ODT were pre-applied for 2 min to allow for complete equilibration in the bath. The solutions of ODT were freshly prepared immediately before use. The concentrations in the figures represent the bath concentrations.

To determine whether activation of PKC plays a role in ODT modulation of SPR-mediated events, oocytes were exposed to a PKC inhibitor, bisindolylmaleimide I (GF109203X) (200 nM) (10), in MBS for 120 min. We then compared the effects of anesthetics on SP-induced Ca^{2+}-activated Cl^- currents in *Xenopus* oocytes expressing SPR between before and after the exposure to GF109203X.

Results were expressed as a percentage of control responses, due to the variable SPR expression rate in oocytes. The control responses were measured before and after application of each test compound to take into account possible shifts in the control currents as recording preceded. The "n" values refer to the number of oocytes studied. Each experiment was performed with oocytes from at least two different frogs. Statistical analyses were performed using either a *t*-test or a one-way ANOVA (analysis of variance).

The tramadol metabolite ODT inhibited the action of

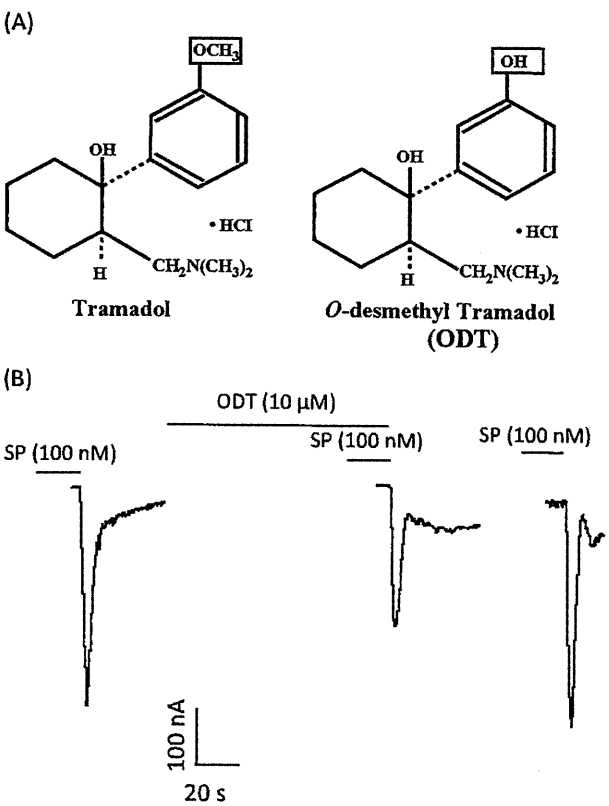

Fig. 1. Effects of *O*-desmethyl tramadol (ODT) on substance P (SP)-stimulated currents in *Xenopus* oocytes expressing SP receptors (SPR). A) Chemical structures of tramadol and *O*-desmethyl tramadol (ODT). B) ODT suppresses the SP-induced Ca^{2+}-activated Cl^- currents in *Xenopus* oocytes expressing SPR. Tracings obtained from a single oocyte expressing SPR show the effect of ODT on currents induced by 100 nM SP. SP was applied for 20 s with or without 2-min ODT treatment.

100 nM SP to 71.0 ± 12.3%, 73.6 ± 9.2%, and 56.7 ± 8.6% of the control at concentrations of 0.1, 1, and 10 μM, respectively (Figs. 1 and 2). After washout of the ODT, the size of SPR-induced currents was reversed to almost the same as the control levels.

We previously reported that treatment with the PKC inhibitor GF109203X (200 nM), which has a Ki value of 20 nM for the inhibition of PKC activity (10), produced the enhancement of the initial Cl^- currents activated by 100 nM SP (4, 5). The control currents before ODT treatment was 35.1 ± 27.6 nA. GF109203X enhanced the currents to 398 ± 86% of the control currents (119 ± 79.6 nA), which was similar to our previous report. The inhibitory effects of ODT on SP-induced currents were observed in the oocytes pretreated with GF109203X (Fig. 3). ODT (10 μM) inhibited the action of 100 nM SP to 52.0 ± 9.7%, while treatment of GF109203X resulted in the action of ODT (10 μM) to 45.9 ± 14.6% of control (Fig. 3), although the effect was not significantly different.

Tramadol undergoes biotransformation in the liver by two metabolic pathways to form five *N*- or *O*-desmethylated metabolites. ODT is one of the five main metabolites of tramadol; and the others are mono-*N*-desmethyl tramadol, di-*N*-desmethyl tramadol, tri-*N*,*O*-desmethyl tramadol, and di-*N*,*O*-desmethyl tramadol. We have previously reported that tramadol had little effect on SPR function (5). In another paper, we reported that a low concentration (under 0.1 μM) of ODT did not suppress SP-induced currents in oocytes expressing the SPR (11). Grond et al. (12) reported the mean ODT concentrations after a 200 mg bolus IV infusion of tramadol and those after patient controlled analgesia with demand doses of 20 mg for 24 h in 92 patients. In our study, the mean concentration of ODT was 84.0 ± 34 ng/mL (approximately 0.3 μM). Sindrup et al. (13) also reported mean ODT concentrations of 5.0 – 122 ng/mL (maximally 0.4 μM) in patients who received 200 – 400 mg of tramadol. In the present study, 0.1 μM and higher concentrations of ODT actually inhibited SP-induced Ca^{2+}-activated Cl^- currents. From the present results, ODT at higher levels,

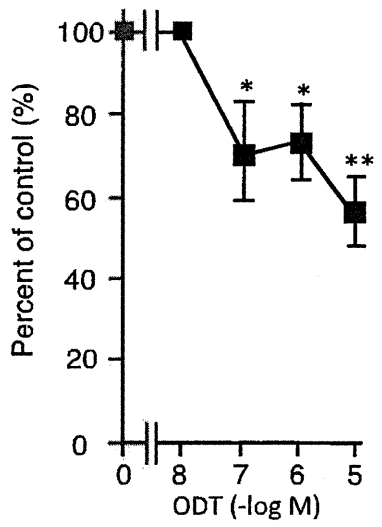

Fig. 2. Concentration–response relationship of *O*-desmethyl tramadol (ODT) on substance P (SP)-induced currents. ODT (10 μM – 10 nM) was applied to the oocytes for 2 min, and then 100 nM of SP was applied for 20 s. Data represent the mean ± S.E.M. of 40 oocytes. $*P < 0.05$ and $**P < 0.01$, compared with the control response using analysis of variance.

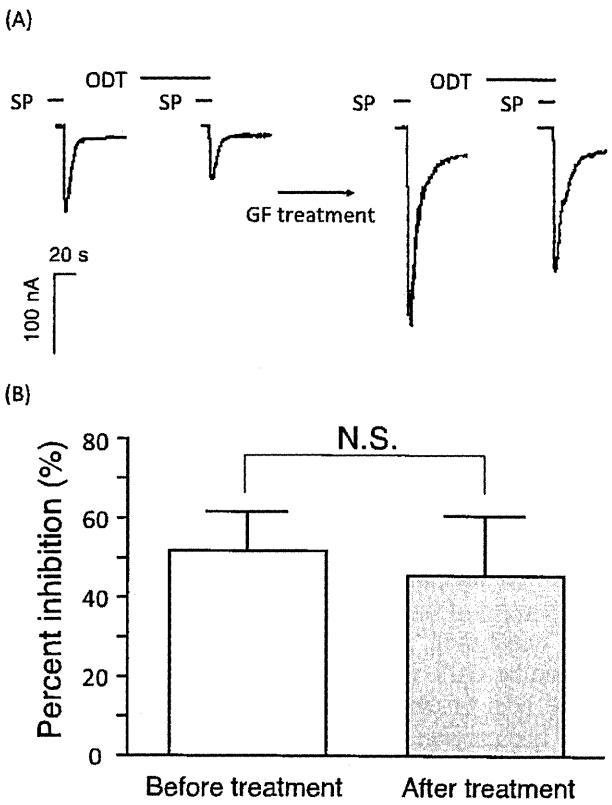

Fig. 3. The effects of GF109203X (protein kinase C inhibitor: PKCI) on inhibition by *O*-desmethyl tramadol (ODT) on substance P (SP)-stimulated currents in *Xenopus* oocytes expressing SP receptors (SPR). A) Tracings obtained from a single oocyte expressing SPR show the effect of ODT on SP (100 nM)-induced currents before and after treatment of PKCI. SP was applied for 20 s with or without 2-min ODT treatment. PKCI was treated for 120 min. B) Comparison of the effects of PKCI on the inhibitory effects of ODT. Oocytes were incubated with 200 nM GF109203X (PKCI) for 120 min. ODT (10 μM) shown was preapplied for 2 min before being co-applied with SP (100 nM) for 20s. "Before treatment" indicates the effects of ODT before application of bisindolylmaleimide. Data represent the mean ± S.E.M. for 10 separate determinations. A paired Student's *t*-test was used for the statistical analysis.

although within the clinically relevant concentrations, would inhibit SPR functions clinically.

The present study raises the question of how ODT inhibits SPR-mediated responses. We have reported that ODT had little effect on the function of muscarinic M_3R, which share the same downstream signaling steps as the SPR following Gq protein activation, expressed in *Xenopus* oocytes. These findings suggest that the inhibitory effect of ODT on the SP-induced Cl^- current is likely due to the inhibition of the SPR before activation of Gq proteins. There is considerable evidence that PKC plays an important role in regulating the function of GPCRs (14) and the functions of some GPCRs are inhibited by PKC activation. We reported that the inhibitory effects of halothane, isoflurane, enflurane, diethyl ether, and ethanol on SP-induced currents were suppressed in oocytes treated with the PKC inhibitor, suggesting that these anesthetics and ethanol inhibit SPR function via activation of PKC. However, in our present experiments, GF109203X did not alter the inhibitory effects of ODT on SPR function, suggesting that PKC may not be involved in the cases of the inhibitory effects of ODT on SPR.

Although much attention has been paid to the μ-opioid receptor and monoamine uptake in the central nervous system as targets for tramadol and ODT, several studies have shown that some GPCRs and ligand-gated ion channels are also targets for tramadol (15). In our present results, the inhibitory effects of ODT seem to be weaker than that on μ-opioid receptors and transporters. Nonetheless, SPR might also be one of the targets for ODT. The inhibitory effects of ODT on SPR might also contribute to the side effects of tramadol. More information about SPR may help to elucidate the role of SPR in the mechanisms of tramadol activity.

In conclusion, we demonstrated that the tramadol metabolite ODT inhibited SPR function. Our findings might help to elucidate the pharmacological basis of ODT and provide a better understanding of its neuronal action and the antinociceptive effects of tramadol. More definitive studies, such as the use of the SPR knockout mouse model, would be required.

Acknowledgments

This work was supported by Grants-in-Aid for Scientific Research from the Ministry of Education, Culture, Sports, Science, and Technology of Japan (K.M., T.Y., Y.U.) and the Health and Labor Sciences Research Grants for 3rd Term Comprehensive 10-year Strategy for Cancer Control (Y.U.).

References

1 De Koninck Y, Henry JL. Substance P-mediated slow excitatory postsynaptic potential elicited in dorsal horn neurons in vivo by noxious stimulation. Proc Natl Acad Sci U S A. 1991;88:11344–11348.
2 Willis WD. Role of neurotransmitters in sensitization of pain responses. Ann N Y Acad Sci. 2001;933:142–156.
3 De Felipe C, Herrero JF, O'Brien JA, Palmer JA, Doyle CA, Smith AJ, et al. Altered nociception, analgesia and aggression in mice lacking the receptor for substance P. Nature. 1998;392:394–397.
4 Minami K, Shiraishi M, Uezono Y, Ueno S, Shigematsu A. The inhibitory effects of anesthetics and ethanol on substance P receptors expressed in Xenopus oocytes. Anesth Analg. 2002;94:79–83.
5 Okamoto T, Minami K, Uezono Y, Ogata J, Shiraishi M, Shigematsu A, et al. The inhibitory effects of ketamine and pentobarbital on substance p receptors expressed in Xenopus oocytes. Anesth Analg. 2003;97:104–110.
6 Hara K, Minami K, Sata T. The effects of tramadol and its metabolite on glycine, gamma-aminobutyric acidA, and N-methyl-D-aspartate receptors expressed in Xenopus oocytes. Anesth Analg. 2005;100:1400–1405.
7 Jesse CR, Nogueira CW. Evidence for the involvement of glutamatergic and neurokinin 1 receptors in the antinociception elicited by tramadol in mice. Pharmacology. 2010;85:36–40.
8 Nakamura M, Minami K, Uezono Y, Horishita T, Ogata J, Shiraishi M, et al. The effects of the tramadol metabolite O-desmethyl tramadol on muscarinic receptor-induced responses in Xenopus oocytes expressing cloned M1 or M3 receptors. Anesth Analg. 2005;101:180–186.
9 Sanna E, Dildy-Mayfield JE, Harris RA. Ethanol inhibits the function of 5-hydroxytryptamine type 1c and muscarinic M1 G protein-linked receptors in Xenopus oocytes expressing brain mRNA: role of protein kinase C. Mol Pharmacol. 1994;45:1004–1012.
10 Toullec D, Pianetti P, Coste H, Bellevergue P, Grand-Perret T, Ajakane M, et al. The bisindolylmaleimide GF 109203X is a potent and selective inhibitor of protein kinase C. J Biol Chem. 1991;266:15771–15781.
11 Ogata J, Minami K, Uezono Y, Okamoto T, Shiraishi M, Shigematsu A, et al. The inhibitory effects of tramadol on 5-hydroxytryptamine type 2C receptors expressed in Xenopus oocytes. Anesth Analg. 2004;98:1401–1406.
12 Grond S, Meuser T, Uragg H, Stahlberg HJ, Lehmann KA. Serum concentrations of tramadol enantiomers during patient-controlled analgesia. Br J Clin Pharmacol. 1999;48:254–257.
13 Sindrup SH, Madsen C, Brosen K, Jensen TS. The effect of tramadol in painful polyneuropathy in relation to serum drug and metabolite levels. Clin Pharmacol Ther. 1999;66:636–641.
14 Minami K, Gereau RW 4th, Minami M, Heinemann SF, Harris RA. Effects of ethanol and anesthetics on type 1 and 5 metabotropic glutamate receptors expressed in Xenopus laevis oocytes. Mol Pharmacol. 1998;53:148–156.
15 Minami K, Uezono Y, Ueta Y. Pharmacological aspects of the effects of tramadol on G-protein coupled receptors. J Pharmacol Sci. 2007;103:253–260.

Neuropharmacology 61 (2011) 1265–1274

Contents lists available at SciVerse ScienceDirect

Neuropharmacology

journal homepage: www.elsevier.com/locate/neuropharm

Transcriptional up-regulation of cell surface $Na_V1.7$ sodium channels by insulin-like growth factor-1 via inhibition of glycogen synthase kinase-3β in adrenal chromaffin cells: enhancement of $^{22}Na^+$ influx, $^{45}Ca^{2+}$ influx and catecholamine secretion

Toshihiko Yanagita [a,*], Shinya Satoh [a], Yasuhito Uezono [b], Kiyotaka Matsuo [c], Takayuki Nemoto [a], Toyoaki Maruta [a], Norie Yoshikawa [a], Tomomi Iwakiri [d], Kouichiro Minami [e], Manabu Murakami [a]

[a] Department of Pharmacology, Miyazaki Medical College, University of Miyazaki, 5200 Kihara Kiyotake, Miyazaki 889-1692, Japan
[b] Cancer Pathophysiology Division, National Cancer Center Research Institute, Tokyo 104-0045, Japan
[c] Department of Pharmacology, Nagasaki University Graduate School of Biomedical Sciences, Nagasaki 852-8523, Japan
[d] Department of Pharmacy, Miyazaki Medical College, University of Miyazaki, Miyazaki 889-1692, Japan
[e] Department of Anesthesiology and Critical Care Medicine, Jichi Medical University, Tochigi 329-0483, Japan

ARTICLE INFO

Article history:
Received 20 May 2011
Received in revised form
14 July 2011
Accepted 20 July 2011

Keywords:
Na^+ channel
$Na_V1.7$
Insulin-like growth factor-1
Glycogen synthase kinase-3β
Up-regulation
Chromaffin cell
Catecholamine secretion

ABSTRACT

Insulin-like growth factor-1 (IGF-1) plays important roles in the regulation of neuronal development. The electrical activity of Na^+ channels is crucial for the regulation of synaptic formation and maintenance/repair of neuronal circuits. Here, we examined the effects of chronic IGF-1 treatment on cell surface expression and function of Na^+ channels. In cultured bovine adrenal chromaffin cells expressing $Na_V1.7$ isoform of voltage-dependent Na^+ channels, chronic IGF-1 treatment increased cell surface [^{3}H]saxitoxin binding by 31%, without altering the Kd value. In cells treated with IGF-1, veratridine-induced $^{22}Na^+$ influx, and subsequent $^{45}Ca^{2+}$ influx and catecholamine secretion were augmented by 35%, 33%, 31%, respectively. Pharmacological properties of Na^+ channels characterized by neurotoxins were similar between nontreated and IGF-1-treated cells. IGF-1-induced up-regulation of [^{3}H]saxitoxin binding was prevented by phosphatydil inositol-3 kinase inhibitors (LY204002 or wortmannin), or Akt inhibitor (Akt inhibitor IV). Glycogen synthase kinase-3 (GSK-3) inhibitors (LiCl, valproic acid, SB216763 or SB415286) also increased cell surface [^{3}H]saxitoxin binding by ~33%, whereas simultaneous treatment of IGF-1 with GSK-3 inhibitors did not produce additive increasing effect on [^{3}H]saxitoxin binding. IGF-1 (100 nM) increased Ser^{437}-phosphorylated Akt and Ser^9-phosphorylated GSK-3β, and inhibited GSK-3β activity. Treatment with IGF-1, LiCl or SB216763 increased protein level of Na^+ channel α-subunit; it was prevented by cycloheximide. Either treatment increased α-subunit mRNA level by ~48% and accelerated α-subunit gene transcription by ~30% without altering α-subunit mRNA stability. Thus, inhibition of GSK-3β caused by IGF-1 up-regulates cell surface expression of functional Na^+ channels via acceleration of α-subunit gene transcription.

1. Introduction

Insulin-like growth factor-1 (IGF-1) and its receptors are widely distributed throughout the nervous system during development, and IGF-1 has an important role in normal brain development, promoting neuronal growth, cellular proliferation and differentiation (Arsenijevic and Weiss, 1998; Connor and Dragunow, 1998; Torres-Aleman, 2010). In addition, IGF-1 has neuroprotective effects against hypoxia/ischemia-induced neuronal injury, neurodegenerative disease, and infectious neuronal disorders (Torres-Aleman, 2010; Trejo et al., 2004; Ying Wang et al., 2003).

Most of the physiological effects of IGF-1 are mediated by the IGF-1 receptor which, after ligand binding-induced autophosphorylation, associates with specific adaptor proteins and activates different second messengers. The activated receptor typically stimulates one or both of two cascades, (1) the Ras~mitogen-activated protein kinase (MAPK)/extracellular signal-regulated kinase (ERK) kinase (MEK)~ERK cascade, via the adaptor protein SHC, or (2) the phosphatydil inositol-3 kinase (PI3K)~Akt cascade, via insulin receptor substrate (IRS) (Bondy and Cheng, 2004; LeRoith

* Corresponding author. Tel.: +81 985 85 1786; fax: +81 985 84 2776.
E-mail address: yanagita@med.miyazaki-u.ac.jp (T. Yanagita).

0028-3908/$ – see front matter © 2011 Elsevier Ltd. All rights reserved.
doi:10.1016/j.neuropharm.2011.07.029

and Roberts, 2003). Activated Akt phosphorylates/inhibits glycogen synthase kinase-3 (GSK-3), and phosphorylates/activates mammalian target of rapamycin (mTOR) (Nemoto et al., 2010b). GSK-3 is one of the key molecules of neurotrophic and neuroprotective effects of IGF-1, insulin, lithium and valproic acid (VPA) (Gurvich and Klein, 2002; Jope, 2003). GSK-3, a serine/threonine protein kinase, is constitutively active in nonstimulated cells, causing phosphorylation and inactivation/degradation of signaling molecules (e.g., glycogen synthase), transcription factors (e.g., β-catenin), translation initiation factor eIF2B, and structural proteins (e.g., tau) (Jope and Johnson, 2004). GSK-3 consists of α and β isoforms and its activity is inhibited by therapeutic concentration of lithium or VPA (Ryves and Harwood, 2001; Gurvich and Klein, 2002).

It has become increasingly evident that coordinately regulated cell surface expression and electrical activity of Na^+ channels play crucial roles in the regulation of axon competition, axon pathfindings, synaptic formation, and maintenance and repair of neuronal circuits (Hanson and Landmesser, 2004; Hua et al., 2005; Xu and Shrager, 2005). In contrast, dysregulated expression and activity of Na^+ channels are associated with hypoxia/ischemia-induced cell injury (Urenjak and Obrenovitch, 1996), seizure (Xia et al., 2000), fatal cardiac arrhythmia (Catterall, 2000) and intolerable pain (Waxman et al., 2000). To understand the molecular basis for these physiological and pathological events, it is essential to explore the mechanisms whereby the expression and function of cell surface Na^+ channels are regulated.

Na^+ channel consists of the principal α-subunit, with or without β_1- to β_4-subunit (Isom, 2002; Catterall et al., 2005). The nine α-subunits ($Na_V1.1$-$Na_V1.9$) arise from nine different genes (SCN1A-SCN5A and SCN8A-SCN11A) (Catterall et al., 2005; Klugbauer et al., 1995; Toledo-Aral et al., 1997). Different α-subunits have distinct electrophysiological and pharmacological properties. The β-subunits are type 1 transmembrane proteins containing a single transmembrane segment, and interact with extracellular (e.g. neurofascin) and intracellular proteins (e.g. ankyrin), regulating gating kinetics and cell surface targeting of Na^+ channel (Catterall et al., 2005; Isom, 2002).

In adrenal chromaffin cells (embryologically derived from the neural crest), α-subunit isoform of Na^+ channels is $Na_V1.7$ [the tetrodotoxin (TTX)/saxitoxin (STX)-sensitive human neuroendocrine type Na^+ channel α-subunit (hNE-Na)] (Klugbauer et al., 1995; Catterall et al., 2005; Wada et al., 2008). In cultured bovine adrenal chromaffin cells, cell surface expression of $Na_V1.7$ is up- and down-regulated by extra- and intra-cellular signalings. Activation of protein kinase C (PKC)-ε (Yanagita et al., 1999, 2000) and ERK (Yanagita et al., 2003) destabilized $Na_V1.7$ mRNA, and activation of PKC-α (Yanagita et al., 1999, 2000) promoted internalization of $Na_V1.7$. Protein kinase A (Yuhi et al., 1996) promoted cell surface externalization of $Na_V1.7$. In addition, several bioactive signaling molecules and therapeutic drugs which would be expected as neuroprotective drugs [Lithium (Yanagita et al., 2009), lysophosphatidic acid (Maruta et al., 2008), insulin (Yamamoto et al., 1996), VPA (Yamamoto et al., 1997), cyclosporin A, FK506 (Shiraishi et al., 2001), and carvedilol (Kajiwara et al., 2002)] up-regulated cell surface Na^+ channels via multiple mechanisms. In the present study, we found that chronic IGF-1 treatment accelerated $Na_V1.7$ α-subunit gene transcription and up-regulated cell surface expression of $Na_V1.7$ via inhibition of GSK-3β, thereby resulting in the enhancement of Na^+ influx, Ca^{2+} channel gating and catecholamine secretion.

2. Materials and methods

2.1. Materials

Eagle's minimum essential medium was from Nissui Seiyaku (Tokyo, Japan). IGF-1 was from PeproTech (London UK). Calf serum and TRIzol reagent were from Invitrogen Corp. (Carlsbad, CA USA). Actinomycin D, cytosine arabinoside, lithium chloride (LiCl), TTX, α-scorpion venom (Leiurus quinquestriatus quinquestriatus), β-scorpion venom (Centruroides sculpturatus), and ouabain were from Sigma (St. Louis, MO, USA). Ptychodiscus brevis toxin-3 (PbTx-3) was from Latoxan, Westbury, (N.Y., USA). Phenylmethylsulfonyl fluoride, leupeptin, aprotinin, sodium orthovanadate, sodium fluoride, Nonidet P-40, Tween-20, and sodium deoxycholate were from Nacalai Tesque (Kyoto, Japan). SB216763 and SB415286 were from Tocris Cookson Ltd. (Avonmouth UK). PD98059, wortmannin, LY294002, Akt inhibitor IV and rapamycin were from Calbiochem (San Diego, CA, USA). Oligotex-dT30 (Super) and mini Quick Spin RNA Columns were from Roche Diagnostics (Tokyo, Japan). BcaBEST labeling kit, and Non-interfering protein assay kit were from Takara (Kyoto, Japan). Rabbit polyclonal antibody against $Na_V1.7$ Na^+ channel α-subunit was from Alomone Labs Ltd. (Jerusalem, Israel). Mouse monoclonal antibody against Akt, and rabbit polyclonal antibodies against IGF-1 receptor β-subunit and insulin receptor β-subunit were from Santa Cruz Biotechnology (Santa Cruz. CA, USA). Mouse monoclonal antibodies against GSK-3β and phosphotyrosine (PY20) were from BD biosciences (San Jose, CA, USA). Rabbit polyclonal antibodies against phosho-GSK-3β (Ser^9) and phospho-Akt (Ser^{473}) were from Cell Signaling Technology (Beverly, MA, USA). RQ1 RNase-Free DNase, proteinase K, and U0126 were from Promega (Madison, WI, USA). [^{3}H]STX (20-40 Ci/mmol), [α-^{32}P]dCTP (>3000 Ci/mmol), [α-^{32}P]UTP (800 Ci/mmol), [γ-^{32}P]ATP (~3000 Ci/mmol), Hybond-N$^+$, Hybond-P, ECL Plus Western Blotting Detection Reagents, and Rapid-hyb buffer were from Amersham Biosciences (Buckinghamshire, UK). cDNA for human glyceraldehyde 3-phosphate dehydrogenase (GAPDH) was from Clontech (Palo Alto, CA, USA). Can Get Signal was from Toyobo (Osaka, Japan). Phospho-glycogen syntase peptide-2 (GSK-3 substrate peptide) was from Upstate Biotechnology, Inc. (Lake Placid, NY, USA). Plasmid Bluescript II (pBII) was from Stratagene (La Jolla, CA, USA). Plasmids containing hNE-Na ($Na_V1.7$) cDNA (Klugbauer et al., 1995), and rat brain Na^+ channel β_1-subunit cDNA (Oh and Waxman, 1994) were generously donated by Drs. F. Hofmann (Technischen Universität München), and Y. Oh (University of Alabama), respectively.

2.2. Primary culture of adrenal chromaffin cells and drug treatment

Isolated bovine adrenal chromaffin cells were cultured (4×10^6/dish, Falcon; 35 mm in diameter) under 5% CO_2/95% air in a CO_2 incubator in Eagle's minimum essential medium containing 10% calf serum, and 3 μM cytosine arabinoside to suppress the proliferation of nonchromaffin cells (Yamamoto et al., 1996). Three days after plating, the cells were exposed to test compounds for up to 72 h. Test compounds were dissolved in distilled H_2O or dimethyl sulfoxide (DMSO), the final concentration of DMSO in the test medium being 0.25%. Treatment of chromaffin cells with 0.25% DMSO for 72 h did not alter [^{3}H]STX binding, compared with nontreated cells. When chromaffin cells were purified by differential plating (Yamamoto et al., 1996), relative abundance of α- and β_1-subunit mRNAs/GAPDH mRNA was similar between conventional and purified adrenal chromaffin cells.

2.3. [^{3}H]STX binding

Cells were washed with ice-cold Krebs–Ringer phosphate (KRP) buffer (mM) (154 NaCl, 5.6 KCl, 1.1 $MgSO_4$, 2.2 $CaCl_2$, 0.85 NaH_2PO_4, 2.15 Na_2HPO_4, 5 glucose, and 0.5% bovine serum albumin, pH 7.4), and incubated with 1–25 nM [^{3}H]STX in 1 ml KRP buffer at 4 °C for 15 min in the absence (total binding) and presence (nonspecific binding) of 1 μM TTX (Yamamoto et al., 1996; Yanagita et al., 1999, 2000; Yuhi et al., 1996). The cells were washed, and solubilized in 10% Triton X-100, and counted for radioactivity. Specific binding was calculated as the total binding minus nonspecific binding.

2.4. $^{22}Na^+$ influx, $^{45}Ca^{2+}$ influx, and catecholamine secretion

$^{22}Na^+$ influx was measured by incubating cells with 2 μCi $^{22}NaCl$ in culture medium or KRP buffer at 37 °C for 5 min without or with veratridine, α-scorpion venom, β-scorpion venom, PbTx-3, and ouabain, and for 1 min without or with nicotine or high K^+ solution. To measure $^{45}Ca^{2+}$ influx and catecholamine secretion, cells were incubated with 2 μCi $^{45}CaCl_2$ for 5 min with or without veratridine in KRP buffer, or for 1 min without or with nicotine or high K^+ solution. Incubation medium was saved into a test tube for catecholamine assay by HPLC, and the cells were washed, solubilized and counted for radioactivity (Yamamoto et al., 1996).

2.5. Western blot analysis of Akt, phosporylated Akt, GSK-3β, phosporylated GSK-3β, and $Na_V1.7$ Na^+ channel α-subunit

Cells were washed with ice-cold Ca^{2+}-free phosphate-buffered saline (PBS), and solubilized at 95 °C for 3 min in 500 μl of 2× SDS electrophoresis sample buffer. Total quantity of cellular proteins was measured by Non-interfering protein assay kit. The same amount of protein (20 μg/each lane) was separated by sodium dodecyl sulfate (SDS) −7.5% or −12% polyacrylamide gel electrophoresis (PAGE), and transferred onto a polyvinylidene difluoride membrane. The membrane was preincubated at room temperature 1% BSA in Tween-Tris-buffered saline [10 mM Tris–HCl (pH 7.4), 150 mM NaCl and 0.1% Tween-20], then reacted overnight at 4 °C with antibodies against Akt, Ser^{473}-phosphorylated Akt, GSK-3β, Ser^9-phosphorylated GSK-3β, and

$Na_V1.7$ Na^+ channel α-subunit. The membrane was washed three times and incubated with horseradish peroxidase-conjugated anti-rabbit IgG or anti-mouse IgG for 1 h. Reaction buffer of 1st and 2nd antibodies were diluted by Can Get Signal solutions. Immunoreactive proteins on the membrane were visualized by the enhanced chemiluminescent detection system ECL Plus (Amersham Biosciences), and quantified by a luminoimage LAS-3000 plus analyzer (Fuji Film, Tokyo). The membrane was rinsed at 60 °C for 30 min with stripping buffer [100 mM 2-mercaptoethanol, 2% SDS, and 62.5 mM Tris–HCl (pH 6.7)] to remove phospho-specific antibody, and used for reprobing with another antibody.

2.6. Immunoprecipitation of GSK-3β and GSK-3β activity assay

Cells were lysed on ice for 15 min in 1 ml of the lysis buffer [50 mM Tris–HCl (pH 7.4), 150 mM NaCl, 1% Nonidet P-40, 0.5% sodium deoxycholate, 1 mM phenylmethylsulfonyl fluoride, 10 mM EDTA, 20 μg/ml aprotinin, 10 μg/ml leupeptin, 100 mM sodium fluoride and 10 mM sodium orthovanadate], and insoluble cell debris was removed by centrifugation at 12,000 g for 10 min. The cell lysate was precleared with protein A-agarose and then incubated with an anti-GSK-3β antibody (1 μg) and protein A-agarose at 4 °C for 3 h. After incubation, proteins bound to the antibody/protein A-agarose complex were precipitated by centrifugation at 12,000 g for 10 min and washed three times with the lysis buffer.

GSK-3β activity assay was performed as previously described (Takahashi-Yanaga et al., 2003). In brief, immunoprecipitated GSK-3β samples were washed twice with lysis buffer and twice with a kinase assay buffer (20 mM Tris/HCl, pH 7.4, 5 mM $MgCl_2$, and 1 mM dithiothreitol). Kinase activity was measured by immunoprecipitated GSK-3β with 50 μl of kinase assay buffer containing 250 μM ATP, 5 μCi of [γ-^{32}P]ATP, and 10 μM GSK-3 substrate peptide. The samples were incubated at 30 °C for 30 min, and the reaction was terminated by adding 10 μl of 50% trichloroacetic acid. Samples were then centrifuged at 15,000 rpm for 5 min, and 40 μl of supernatant was spotted on P81 phosphocellulose filter paper (Whatman). The filters were washed five times with 0.75% phosphoric acid and twice with acetone and analyzed by scintillation counting.

2.7. Immunoprecipitation and immunoblot analysis of tyrosine-phosphorylated IGF-1 receptor and insulin receptor

Cell lysates in the lysis buffer [50 mM Tris–HCl (pH 7.4), 150 mM NaCl, 1% Nonidet P-40, 0.5% sodium deoxycholate, 1 mM phenylmethylsulfonyl fluoride, 10 mM EDTA, 20 μg/ml aprotinin, 10 μg/ml leupeptin, 100 mM sodium fluoride and 10 mM sodium orthovanadate] were subjected to immunoprecipitation with IGF-1 receptor antibody or insulin receptor antibody. The immunoprecipitates were reacted with protein A-agarose or protein G-agarose, washed with lysis buffer, finally suspended in 2x SDS electrophoresis sample buffer at 98 °C, and centrifuged; the resultant supernatant was separated by 7.5% SDS-PAGE and transferred to membrane for immunoblot analysis. To measure IGF-1- or insulin-induced tyrosine phosphorylation of IGF-1 receptor and insulin receptor, cells were treated at 37 °C with or without 10–100 nM IGF-1 or insulin for 10 min in the culture medium, washed twice with KRP buffer, and solubilized in the lysis buffer; the cell lysates were subjected to immunoprecipitation with IGF-1 receptor β-subunit or insulin receptor β-subunit antibody.

For immunoblot analysis, the membrane was preincubated with 1% bovine serum albumin in the Tween-Tris-buffered solution, and reacted overnight at 4 °C in Can Get Signal Solution-1 with phospho-tyrosine specific antibody. The immunoreactive bands were labeled with horseradish peroxidase-conjugated anti-rabbit antibody and analyzed by a luminoimage LAS-3000 analyzer. The membrane was rinsed at 60 °C for 30 min with stripping buffer (100 mM 2-mercaptoethanol, 2% sodium dodecyl sulfate, and 62.5 mM Tris–HCl [pH 6.7]) to remove phosphotyrosine specific antibody, and used for reprobing with another antibody.

2.8. Northern blot

Total cellular RNA was isolated from the cells by acid guanidine thiocyanate phenol-chloroform extraction using TRIzol reagent. Poly $(A)^+$ RNA was purified by Oligotex-dT30 (Super), electrophoresed on 1% agarose gel containing 6.3% formaldehyde in the buffer [40 mM 3-(N-morpholino) propanesulfonic acid, pH 7.2, 0.5 mM EDTA, and 5 mM sodium citrate], transferred to a nylon membrane (Hybond-N^+, Amersham) in 20× saline-sodium citrate (SSC; 1× SSC = 0.15 M NaCl and 0.015 M sodium citrate) overnight, and cross-linked using a UV cross-linker (Funakoshi, Tokyo, Japan).

Plasmids containing $Na_V1.7$ cDNA, and β_1-subunit cDNA were digested, respectively, with MunI, and with SacII plus HindIII to obtain nucleotide (nt) fragments for α-subunit (nt 1365–2948), and β_1-subunit (nt 457–790). These cDNA fragments and GAPDH cDNA (1.1 kbp) were labeled with [α-^{32}P]dCTP using BcaBEST labeling kit. The membrane was prehybridized, and then hybridized with $Na_V1.7$ probe at 65 °C for 4 h in Rapid hyb buffer. It was washed in 0.2× SSC containing 0.1% SDS for 30 min twice, and subjected to autoradiography. The same membrane was successively hybridized with probes for β_1-subunit, and then GAPDH, after being washed with 0.1% SDS at 100 °C to remove the former probe. Autoradiogram was quantified by a bioimage analyzer BAS 2000.

2.9. Nuclear run-on assay

Cells were washed twice with ice-cold PBS, dislodged, and centrifuged at 500 × g for 5 min. Cell pellets were suspended in buffer A (10 mM Tris–HCl, pH 7.4, 10 mM NaCl, 3 mM $MgCl_2$, and 0.4% Nonidet P-40), treated on ice for 5 min, and centrifuged at 500 g for 5 min. Nuclear pellets were washed with buffer A, and suspended in buffer B (50 mM Tris–HCl, pH 8.3, 40% glycerol, 5 mM $MgCl_2$, and 0.1 mM EDTA). Nuclei (1.2×10^7/100 μl) were incubated at 30 °C for 30 min with 100 μl buffer C (10 mM Tris–HCl, pH 8.0, 5 mM $MgCl_2$, 200 mM KCl, 2 mM dithiothreitol, 0.5 mM of each ATP, CTP, GTP, and 200 μCi [α-^{32}P]UTP), after which DNA was digested by exposing to 2U RQ1 RNase-Free DNase for 10 min at 30 °C. Proteins were digested in 200 μl buffer D (20 mM Tris–HCl, pH 7.4, 10 mM EDTA, 20% SDS, and 200 μg/ml proteinase K) at 50 °C for 1 h. Newly-transcribed RNAs were extracted by using TRIzol reagent, dissolved in TE (10 mM Tris–HCl, pH 7.5 and 1 mM EDTA), and purified by mini Quick Spin RNA Columns. ^{32}P-Labeled RNAs (5×10^6 cpm/ml) were hybridized overnight at 70 °C in Rapid-hyb buffer with nylon membrane immobilizing 10 μg pBII alone, and pBII containing $Na_V1.7$ cDNA or GAPDH cDNA. $Na_V1.7$ cDNA fragment (nt 1–2253) was liberated by digesting $Na_V1.7$ plasmid (Klugbauer et al., 1995) with KpnI and BglII, and subcloned into pBII (Yanagita et al., 1999). The membrane was sequentially washed in 2× SSC containing 0.1% SDS at 65 °C for 15 min, 2× SSC containing 10 μg/ml RNase A at 37 °C for 10 min, 0.2× SSC containing 0.1% SDS at 65 °C for 10 min, and then subjected to autoradiography.

2.10. Statistical methods

[^{3}H]STX binding, $^{22}Na^+$ influx, $^{45}Ca^{2+}$ influx and catecholamine secretion were measured in triplicate, and all experiments were repeated at least three times (mean ± SE). Significance ($p < 0.05$) was determined by t-test or one-way analysis of variance with post hoc mean comparison by the Newman–Keuls multiple range test.

3. Results

3.1. Concentration- and time-dependent increase of cell surface [^{3}H]STX binding by chronic treatment with IGF-1: prevention by cycloheximide and actinomycin D

To evaluate the effect of chronic IGF-1 treatment on the cell surface density of Na^+ channels, adrenal chromaffin cells were treated with or without 1–1000 nM IGF-1 for 24 h, and [^{3}H]STX binding was assayed (Fig. 1A). IGF-1 increased cell surface [^{3}H]STX binding in a concentration-dependent manner with the EC_{50} value of 18 nM. The increase in the binding became evident within 12 h after treatment with 100 nM IGF-1, reaching the almost maximal increase of 31% at 72 h (Fig. 1B). The increasing effect of IGF-1 was reversible, because washing the cells at 24 h with culture medium followed by an additional 24 h incubation without IGF-1 restored [^{3}H]STX binding to 106% of the value for nontreated cells (data not shown). Scatchard plot analysis (Fig. 1C) revealed that IGF-1 treatment (100 nM, 24 h) significantly raised the B_{max} values from 59.6 ± 6.1 to 77.2 ± 5.9 fmol/4 × 10^6 cells without altering the K_d values (4.4 ± 0.8 nM, nontreated cells; 4.3 ± 0.9 nM, IGF-1 treated cells; $n = 3$). Because IGF-1-induced up-regulation of [^{3}H]STX binding required chronic (≥12 h) IGF-1 treatment, we examined whether IGF-1-induced up-regulation of [^{3}H]STX binding could require *de novo* synthesis of protein(s). As shown in Fig. 1D, either cycloheximide (10 μg/ml), an inhibitor of protein synthesis, and actinomycin D (10 μg/ml), an inhibitor of RNA synthesis, significantly decreased [^{3}H]STX binding but completely prevented the rise of [^{3}H]STX binding caused by IGF-1.

3.2. Up-regulation of $^{22}Na^+$ influx via Na channels in cells treated with IGF-1: similar pharmacological properties of Na^+ channels between nontreated and IGF-1-treated cells

Neurotoxins that bind to distinct sites at the Na^+ channel are useful probes for characterizing structure and function of Na^+ channels (Cestèle and Catterall, 2000). When cells were stimulated with various concentrations of veratridine, which binds to site 2, segment 6 of domain I (IS6) (Cestèle and Catterall, 2000), veratridine increased $^{22}Na^+$ influx in a concentration-dependent manner.

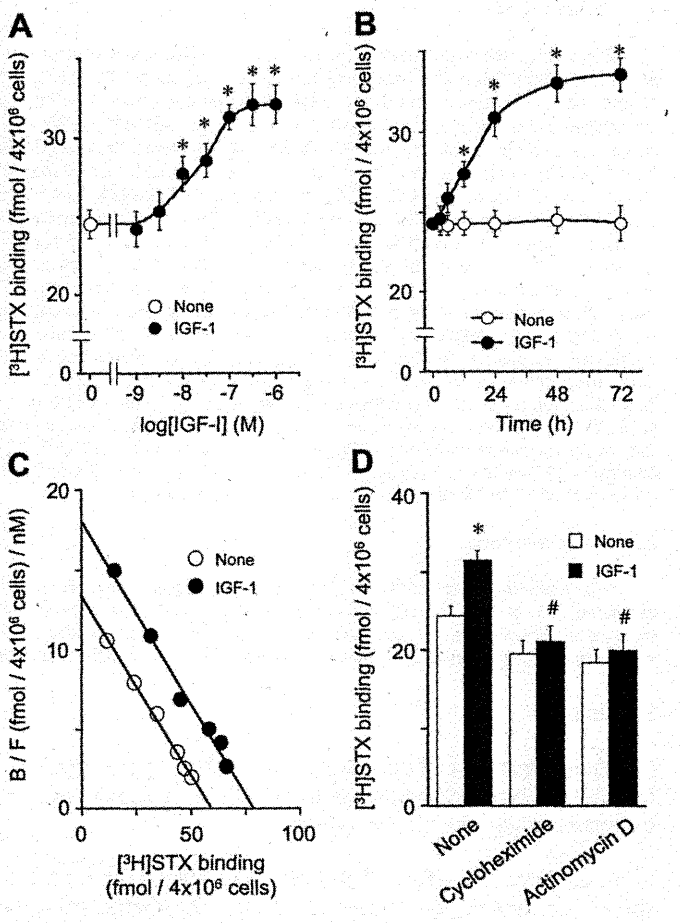

Fig. 1. Concentration- and time-dependent increase of cell surface [^{3}H]STX binding by chronic treatment with IGF-1: prevention by cycloheximide and actinomycin D. (A) Cells were treated with or without indicated concentrations of IGF-1 for 24 h, and subjected to [^{3}H]STX binding. Mean ± S.E.M. ($n = 5$). *$P < 0.05$, compared with non-treated cells. (B) Cells were treated with or without 100 nM IGF-1 for up to 72 h, and subjected to [^{3}H]STX binding assay at the indicated times. Mean ± S.E.M. ($n = 5$). *$P < 0.05$, compared with nontreated cells. (C) Scatchard plot analysis of [^{3}H]STX binding in cells treated with or without 100 nM IGF-1 for 24 h. Data are typical from three independent experiments with similar results. (D) Cells were treated with (IGF-1: closed columns) or without (None: open columns) 100 nM IGF-1 for 24 h in the absence or presence of 10 μg/ml cycloheximide or 10 μg/ml Actinomycin D, and subjected to [^{3}H]STX binding assay. Mean ± S.E.M. ($n = 3$). *$P < 0.05$, compared with cells not treated with IGF-1; #, no significant difference within each cell group.

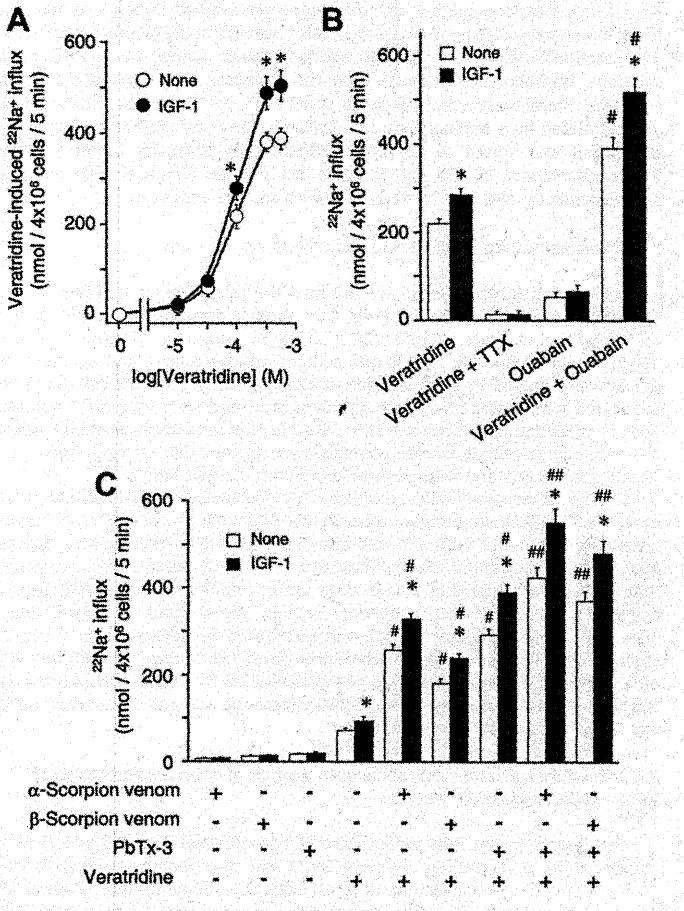

Fig. 2. Up-regulation of $^{22}Na^+$ influx via Na channels in cell treated with IGF-1: pharmacological characterization by neurotoxins. Cells were treated with or without 100 nM IGF-1 for 24 h and washed with KRP buffer; they were exposed to 2 μCi $^{22}NaCl$ for 5 min in the presence or absence of (A) 1–500 μM veratridine, (B) 100 μM veratridine and/or 100 μM ouabain, or 100 μM veratridine and 1 μM TTX, or (C) 30 μM veratridine and/or 0.5 μg/ml α-scorpion venom, 5 μg/ml β-scorpion venom, and 1 μM PbTx-3. Basal $^{22}Na^+$ influx value at 37 °C (nmol/4 × 10^6 cells/5 min) was not changed in cells treated with IGF-1 (18.2 ± 2.7), compared with nontreated cells (17.6 ± 2.9). These basal values are subtracted from the data. Mean ± S.E.M. ($n = 3$). *$P < 0.05$, compared with IGF-1-nontreated cells; #$P < 0.05$, compared with veratridine alone within each IGF-1-nontreated and IGF-1-treated cell group; ##$P < 0.05$, compared with veratridine plus PbTx-3 within each IGF-1-nontreated and IGF-1-treated cell group.

Fig. 2A shows that in cells treated with IGF-1, veratridine-induced $^{22}Na^+$ influx was augmented by 35%, with no change in EC_{50} values of veratridine (81 μM, nontreated cells; 85 μM, IGF-1-treated cells). Fig. 2B shows that veratridine-induced $^{22}Na^+$ influx both in the nontreated cells and the IGF-1-treated cells was abolished by 1 μM TTX, consistent with $Na_V1.7$ being sensitive to the inhibition by TTX/STX (Klugbauer et al., 1995; Catterall et al., 2005). We then characterized pharmacological properties of Na^+ channels by using α-scorpion venom, which binds to site 3 (IS5-S6), β-scorpion venom, which interacts with site 4 (IIS1-S2, IIS3-S4), and PbTx-3, which binds to site 5 (IS6): these toxins enhance veratridine-induced Na^+ influx (Cestèle and Catterall, 2000; Yanagita et al., 2007). α-Scorpion venom, β-scorpion venom, and PbTx-3 caused only a slight increase of $^{22}Na^+$ influx over the basal value, and potentiated veratridine-induced $^{22}Na^+$ influx, by 2.8-, 2.0-, and 4.8-fold, respectively, as reported previously (Yanagita et al., 2007) (Fig. 2C). In addition, PbTx-3 in combination with either α-scorpion venom, or β-scorpion venom augmented veratridine-induced $^{22}Na^+$ influx to a greater extent than did either toxin/venom alone. These toxin-induced potentiations of veratridine-induced $^{22}Na^+$ influx were also observed in the IGF-1 treated cells, as in the nontreated cells (Fig. 2C).

Our previous study showed that Na^+ influx increases the activity of Na^+, K^+-ATPase, whereby Na^+, once it enters chromaffin cells, is continuously pumped out (Yamamoto et al., 1996, 1997). Fig. 2B shows that ouabain at 100 μM, a concentration which totally inhibits the activity of Na^+, K^+-ATPase (Yamamoto et al., 1996, 1997), increased accumulation of $^{22}Na^+$, and it was not changed by IGF-1. In the presence of ouabain, veratridine (100 μM)-induced $^{22}Na^+$ influx occurred to a greater extent in cells treated with IGF-1, compared with nontreated cells.

3.3. *Up-regulation of veratridine-induced (but not high K^+-induced) $^{45}Ca^{2+}$ influx via voltage-dependent Ca^{2+} channels and catecholamine secretion in cells treated with IGF-1*

In adrenal chromaffin cells, our previous studies showed that veratridine-induced Na^+ influx via Na^+ channels is indispensable for the gating of voltage-dependent Ca^{2+} channels, a prerequisite

for exocytic secretion of catecholamines, whereas a high K^+ concentration directly gates voltage-dependent Ca^{2+} channels without stimulating Na^+ influx (Yamamoto et al., 1996, 1997). In the present study, treatment with 100 nM IGF-1 for 24 h enhanced veratridine-induced $^{45}Ca^{2+}$ influx and catecholamine secretion by 33 and 31%, respectively (Fig. 3A and B; veratridine), whereas the same treatment did not alter high K^+ (56 mM)-induced $^{45}Ca^{2+}$ influx and catecholamine secretion (Fig. 3A and B; High K^+).

3.4. IGF-1-induced up-regulation of [^{3}H]STX binding: involvement of PI3K~Akt~GSK-3 pathway

To evaluate the intracellular signaling cascade of increasing effect of IGF-1, we also examined the effects of kinase inhibitors (MEK inhibitors, PI3K inhibitors, Akt inhibitors, mTOR inhibitors and GSK-3 inhibitors) on IGF-1-induced up-regulation of [^{3}H]STX binding (Fig. 4). We have reported that inhibition of ERK by PD98059 or U0126 up-regulated cell surface expression of Na^+ channels via reduction of RNA degradation of α-subunit mRNA in bovine adrenal chromaffin cells (Yanagita et al., 2003). As shown in Fig. 4, either 50 μM PD98059 or 10 μM U0126, *per se*, raised [^{3}H]STX binding by ~28%, but did not prevent IGF-1-induced up-regulation of [^{3}H]STX binding. PI3K inhibitors (100 μM LY294002 and 100 nM wortmannin) and Akt inhibitor (50 μM Akt inhibitor IV), but not mTOR inhibitor (1 μM Rapamycin) prevented IGF-1-induced up-regulation of [^{3}H]STX binding. LiCl and VPA are potent inhibitors for GSK-3β (Ryves and Harwood, 2001; Gurvich and Klein, 2002), and SB216763 and SB415286 are highly selective inhibitors for GSK-3; previous in vitro assay showed that among 25 different classes of serine/threonine and tyrosine kinases examined, SB216763 and SB415286 inhibited only GSK-3β by 96% and 83% at 10 μM (Coghlan et al., 2000). In bovine adrenal chromaffin cells, we have previously reported that inhibition of GSK-3β by LiCl up-regulated cell surface expression of Na^+ channels via acceleration of gene transcription rate of α-subunit (Yanagita et al., 2009). VPA, SB216763 and SB415286 also up-regulated cell surface expression of Na^+ channels in a concentration-dependent manner (Yamamoto et al., 1997; Yanagita et al., 2009). As shown in Fig. 4, GSK-3 inhibitors (20 mM LiCl, 1 mM VPA, 10 μM SB216763 and 10 μM SB415286), *per se*, raised [^{3}H]STX binding by ~33% as reported previously. Simultaneous treatment of IGF-1 with these GSK-3 inhibitors did not produce an additional increasing effect on [^{3}H]STX binding, compared with either treatment alone.

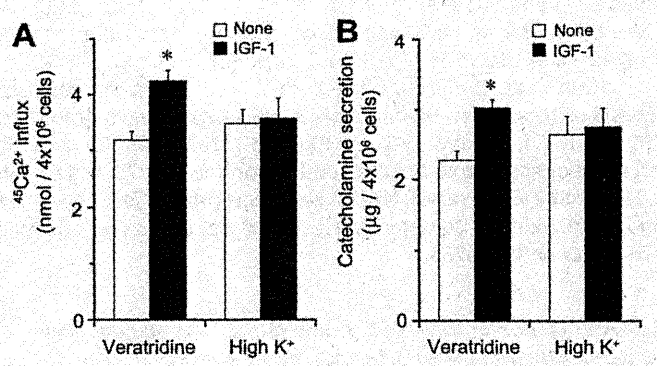

Fig. 3. Up-regulation of veratridine- (but not high K^+-) induced (A) $^{45}Ca^{2+}$ influx and (B) catecholamine secretion in cells treated with IGF-1. Cells treated with (IGF-1: closed columns) or without (None: open columns) 100 nM IGF-1 for 24 h were washed, and incubated with 2 μCi $^{45}CaCl_2$ at 37 °C in the absence or presence of 100 μM veratridine for 5 min in KRP buffer, or in 56 mM high K^+ solution for 1 min. Then, influx of $^{45}Ca^{2+}$ to the cells and catecholamines secreted in the incubation medium were measured. Basal values obtained at 37 °C without veratridine or high K^+ were not changed by IGF-1 treatment, and subtracted. Mean ± SE ($n = 3$). *$p < 0.05$, compared with IGF-1-nontreated cells.

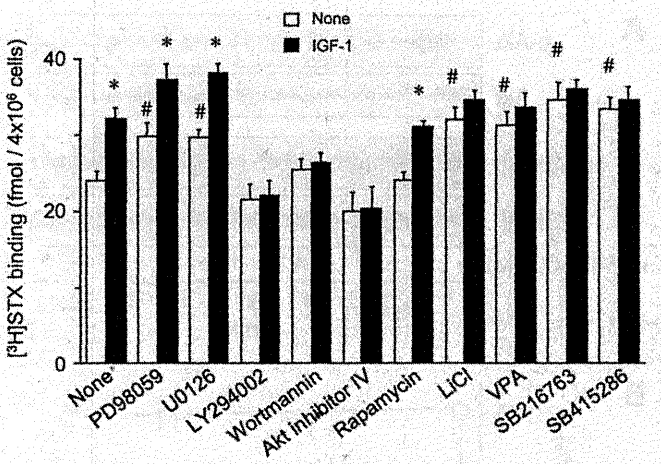

Fig. 4. IGF-1-induced up-regulation of [^{3}H]STX binding: prevention by PI3 K, Akt and GSK-3 inhibitors but not by ERK and mTOR inhibitors. Cells were treated with (IGF-1: closed columns) or without (None: open columns) 100 nM IGF-1 for 24 h in the absence or presence of MEK inhibitor (50 μM PD98059 or 10 μM U0126), PI3K inhibitor (50 μM LY294002 or 100 nM wortmannin), Akt inhibitor (10 μM Akt inhibitor IV), mTOR inhibitor (10 μM rapamycin), or GSK-3 inhibitor (20 mM LiCl, 1 mM VPA, 10 μM SB216763 or 10 μM SB415286), and subjected to [^{3}H]STX binding assay. Mean ± S.E.M. ($n = 3$). *$P < 0.05$, compared with cells not treated with IGF-1 within each cell group; #, $P < 0.05$, compared with cells not treated with IGF-1 and kinase inhibitor.

3.5. IGF-1-induced increase in Ser^{473}-phosphorylated Akt and Ser^9-phosphorylated GSK-3β levels as well as inhibition of GSK-3β

Because increase in [^{3}H]STX binding by IGF-1 was prevented by Akt inhibitor and masked by GSK-3β inhibitor-induced increase in [^{3}H]STX binding, we examined IGF-1-induced Ser^{473}-phosphorylation of Akt as well as Ser^9-phosphorylation and activity of GSK-3β. Cells were treated with or without 100 nM IGF-1 for up to 24 h, Ser^{473}-phosphorylated Akt and Ser^9-phosphorylated GSK-3β were measured by western blot analysis (Fig. 5A). The increase in the phosphorylated Akt and GSK-3β became evident within 1 min after treatment with 100 nM IGF-1, and continued for up to 24 h.

It has been reported that Ser^9-phosphorylation of GSK-3β inhibits GSK-3β activity (Jope, 2003; Jope and Johnson, 2004). We also examined the effect of IGF-1 on the activity of GSK-3β. As shown in Fig. 5B, the maximum inhibition of GSK-3β activity was observed at 1 min after treatment with 100 nM IGF-1, and inhibition of GSK-3β activity was continued for up to 24 h.

3.6. IGF-1-induced phosphorylation of both IGF-1 receptor and insulin receptor, and insulin-induced phosphorylation of insulin receptor but not IGF-1 receptor

Evidence has accumulated that IGF-1 receptor and insulin receptor resemble in the structure and features, and share the signaling cascade (Barbieri et al., 2003). We further examined ligand selectivity of IGF-1 and insulin against both IGF-1 receptor and insulin receptor in bovine adrenal chromaffin cells. IGF-1 (10 and 100 nM) caused tyrosine phosphorylation of both IGF-1 receptor (Fig. 6A, lanes 4 and 5) and insulin receptor (Fig. 6B, lanes 4 and 5) in a concentration-dependent manner. On the other hand, insulin (10 and 100 nM) caused tyrosine phosphorylation of insulin receptor (Fig. 6B, lanes 2 and 3 but not IGF-1 receptor (Fig. 6A, lanes 2 and 3), although very small content of tyrosine

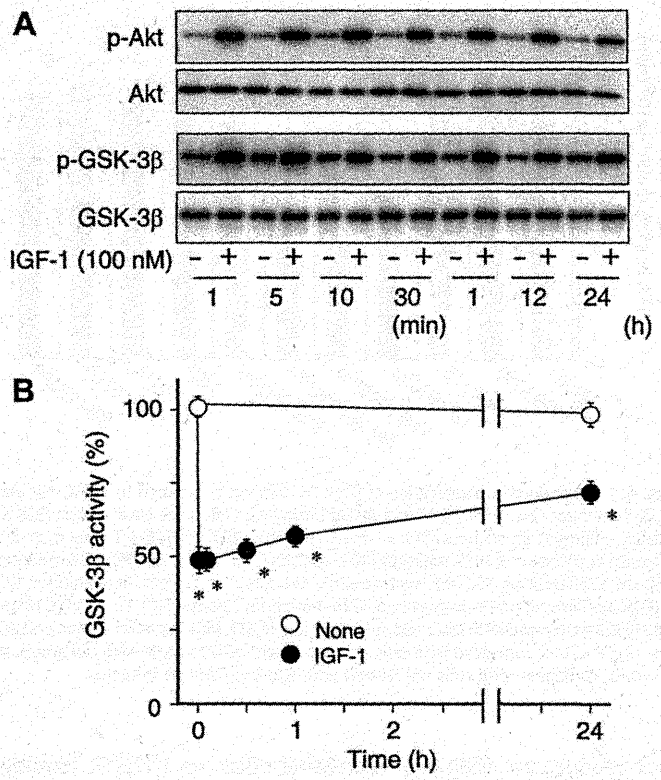

Fig. 5. IGF-1-induced phosphorylation of Ser^{473}-Akt and Ser^{9}-GSK-3β, and inhibition of GSK-3β activity. (A) Cells were treated with or without 100 nM IGF-1 for up to 24 h. The whole-cell lysates were solubilized, size-fractionated by SDS- 7.5% PAGE, and transferred to a membrane for the Western blot analysis of Ser^{473}-phosphorylated Akt, Akt, Ser^{9}-phosphorylated GSK-3β and GSK-3β. (B) Cells were treated with or without 100 nM IGF-1 for the indicated periods, then cells were lysed and immunoprecipitated with anti-GSK-3β antibody and protein A-agarose: these immunoprecipitated GSK-3β samples were subjected to the GSK-3β kinase assay. The relative level of GSK-3β activity is shown. The relative level in untreated cells at 0 h is assigned a value of 100%. Mean ± S.E.M. ($n = 3$). *$P < 0.05$, compared with untreated cells.

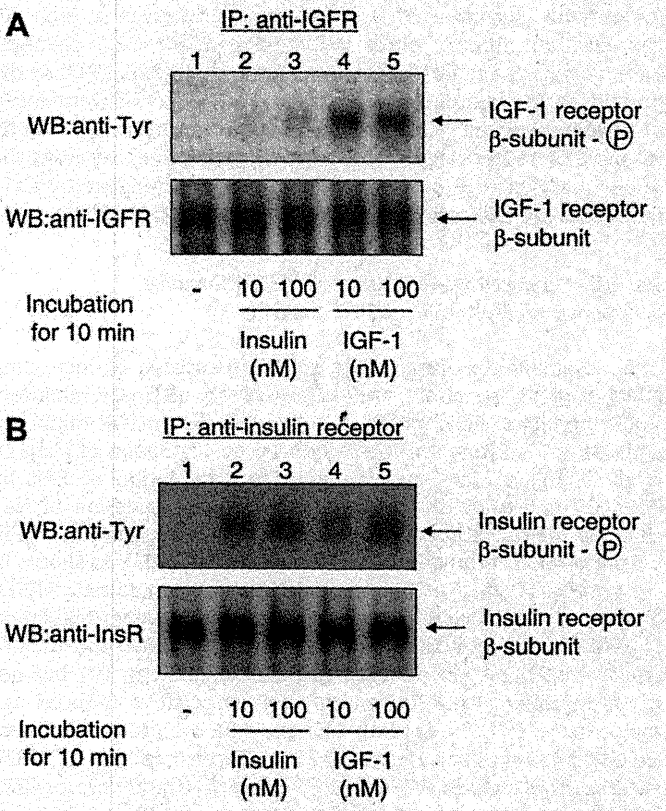

Fig. 6. IGF-1-induced phosphorylation of both IGF-1 receptor and insulin receptor, and insulin-induced phosphorylation of insulin receptor but not IGF-1 receptor. Cells were treated with or without 10 and 100 nM IGF-1 or insulin for 10 min. Cell lysates were subjected to immunoprecipitation (IP) with IGF-1 receptor antibody (A) or insulin receptor antibody (B); the immunoprecipitates were separated by SDS-PAGE, transferred to membrane, and subjected to Western blot (WB) analysis using phosphotyrosine-specific antibody (A, B; upper panel), IGF-1 receptor antibody (A; lower panel) or insulin receptor antibody (B; lower panel). These blots were typical from three independent experiments with similar results.

phosphorylation of IGF-1 receptor was observed only at 100 nM insulin (Fig. 6A, lane 3).

3.7. Up-regulation of $Na_V1.7$ α-subunit (but not $β_1$-subunit) mRNA and $Na_V1.7$ α-subunit protein levels in cells treated with IGF-1

Because IGF-1-induced up-regulation of [^{3}H]STX binding was dependent on the translational event, we examined whether IGF-1 treatment may increases Na^+ channel α- and β-subunit mRNA levels. Among five isoforms of TTX/STX-sensitive Na^+ channel α-subunit ($Na_V1.1$-1.4, and $Na_V1.7$) and four isoforms of Na^+ channel β-subunit ($β_{1-4}$), adrenal chromaffin cells express $Na_V1.7$ α-subunit, and $β_1$- and $β_3$-subunits (Catterall et al., 2005; Brackenbury et al., 2008; Wada et al., 2008; Patino and Isom, 2010). Na^+ channel β-subunits are multifunctional molecules: they can act not only as the modulator of Na^+ channel α-subunit but also as the immunoglobulin superfamily cell adhesion molecules and the signaling molecules that interact with other signaling proteins (Brackenbury et al., 2008; Patino and Isom, 2010). The associated β-subunit isoforms of $Na_V1.7$ are $β_1$- and $β_2$-subunit (Catterall et al., 2005). Therefore, we measured steady-state levels of $Na_V1.7$ α-subunit mRNA and $β_1$-subunit mRNA by Northern blot analysis in cells treated with or without 100 nM IGF-1, 20 mM LiCl, or 10 μM SB216763 (Fig. 7A).

In our present study, $Na_V1.7$ probe hybridized to one major (~9.4 kb) and two minor (~11.0 and ~7.0 kb) transcripts; $β_1$-subunit probe hybridized to a single (~1.5 kb) transcript, as reported previously (Yamamoto et al., 1996, 1997; Yanagita et al., 1999, 2000, 2003, 2009). Levels of α (9.4 kb)- and $β_1$-subunit mRNAs were normalized against that of GAPDH mRNA (Fig. 7B and C). As reported previously, LiCl raised α- (but not $β_1$-) subunit mRNA level. IGF-1 and SB216763 also raised α- (but not $β_1$-) subunit mRNA level by ~23% as early as 6 h, causing the maximum plateau increase of ~48% at 48 h ($t_{1/2} = 7.9$ h and 8.1 h, respectively).

Furthermore, the protein levels of $Na_V1.7$ α-subunit were also measured by western blot analysis in cells treated with or without 100 nM IGF-1, 20 mM LiCl, or 10 μM SB216763 for 24 h in the presence or absence of 10 μg/ml cycloheximide (Fig. 7D and E). IGF-1, LiCl or SB216763 raised $Na_V1.7$ α-subunit protein level by ~35%, and cycloheximide completely prevented the increasing effects of IGF-1, LiCl or SB216763.

3.8. Acceleration of transcription rate of $Na_V1.7$ α-subunit gene by IGF-1: no effect on $Na_V1.7$ α-subunit mRNA stability

Because IGF-1, LiCl and SB216763 raised steady-state level of $Na_V1.7$ α-subunit mRNA, we examined the transcription rate of $Na_V1.7$ α-subunit gene and/or the degradation rate of $Na_V1.7$ α-subunit mRNA. Cells were treated with or without 100 nM IGF-1, 20 mM LiCl or 10 μM SB216763 for 12 h, and the transcription rate of $Na_V1.7$ α-subunit gene was measured by nuclear run-on assay (Yanagita et al., 1999, 2003, 2009). As reported previously, LiCl